Annals of Nuclear Energy 177 (2022) 109300

Contents lists available at ScienceDirect

Annals of Nuclear Energy

journal homepage: www.elsevier.com/locate/anucene

Modelling and simulations of reactor neutron noise induced by mechanical vibrations

A. Vidal-Ferràndiz [a], D. Ginestar [a], A. Carreño [a], G. Verdú [a,*], A. Dokhane [b], V. Verma [b], Y. Perin [c], J. Herb [c], A. Mylonakis [d], C. Demazière [d], P. Vinai [d]

[a] Universitat Politècnica de València, Camino de Vera s/n, 46022 València, Spain
[b] Reactor Physics and Systems Behaviour Laboratory, Paul Scherrer Institut, Villigen, Switzerland
[c] Gesellschaft für Anlagen- und Reaktorsicherheit (GRS) mbH, Boltzmannstraße 14, 85748 Garching, Germany
[d] Division of Subatomic, High Energy and Plasma Physics, Department of Physics, Chalmers University of Technology, SE-412 96, Gothenburg, Sweden

ARTICLE INFO

Article history:
Received 28 February 2022
Received in revised form 4 June 2022
Accepted 20 June 2022

Keywords:
Neutron noise
Fuel assembly vibrations
Neutron diffusion
Frequency domain
Time domain

ABSTRACT

Mechanical vibrations of core internals are among the main perturbations that induce oscillations in the neutron flux field, also known as neutron noise. In this work, different simulation models for the study of the influence of the mechanical vibrations of fuel assemblies on the neutron flux in the reactor core have been discussed. These methodologies employ the diffusion approximation, with or without a previous homogenization model, to simulate the neutron noise in the time or the frequency domain. The diffusion-based approach is expected to be less accurate in the vicinity of the vibrating fuel assemblies, but correct when considering distances larger than a few diffusion lengths away from the perturbation. All methodologies provide consistent results and can reproduce typical features of the neutron noise induced by mechanical vibrations of core components. First, FEMFFUSION can perform simulations in both the time and frequency domains. Second, CORE SIM + can be used to study various neutron noise scenarios in realistic three-dimensional reactor configurations. The third methodology is centred on using commercial codes as CASMO-5, SIMULATE-3 and SIMULATE-3K. This methodology allows time domain simulations of the neutron noise induced by different neutron noise sources in a nuclear reactor. Finally, a model for time-dependent geometry is implemented for the code system ATHLET/QUABOX-CUBBOX employing a cross-section-based approach for encoding water gap width variations at the reflector.

1. Introduction

In the area of core monitoring, detection of reactor perturbations gives the possibility to take proper actions before such problems lead to safety concerns or impact plant availability. The CORTEX project (Demazière et al., 2018), aims at developing an innovative core monitoring methodology that allows detecting anomalies in nuclear reactors, such as excessive vibrations of core internals, flow blockage and coolant inlet perturbations. This methodology is based on using the fluctuations of the neutron flux around its steady state value, known as neutron noise, recorded by in-core and ex-core detectors. The main benefit of this method is that it can be applied on-line without disrupting plant operation. Furthermore, the method is non-intrusive, i.e. no additional perturbation needs to be introduced.

A correlation between the stiffness of fuel assemblies (FA) and neutron noise levels was experimentally demonstrated (Seidl et al., 2015), indicating the direct effect of FA vibrations onto the neutron noise. FA vibrations have been studied from a mechanical point of view in (Park et al., 2003 and Fry et al., 1984). Natural frequencies range from 0.8 Hz to 24.5 Hz depending on the idealized form of bearing and their building materials. The amplitude of the vibration ranges can reach up to 1 mm. However, there can be amplitudes greater than 1 mm in case of synchronous motions.

This work is dedicated to the study of the influence of the mechanical vibrations of Fuel Assemblies (FA) on the neutron flux in nuclear reactors. These mechanical vibrations are among the main reasons that induce reactor neutron noise. To model this effect, different codes and methodologies are explained in

* Corresponding author.
E-mail addresses: anvifer2@upv.es (A. Vidal-Ferràndiz), dginesta@mat.upv.es (D. Ginestar), amcarsan@iqn.upv.es (A. Carreño), gverdu@iqn.upv.es (G. Verdú), abdelhamid.dokhane@psi.ch (A. Dokhane), vasudha.verma75@gmail.com (V. Verma), yann.perin@grs.de (Y. Perin), joachim.herb@grs.de (J. Herb), antonios.mylonakis@chalmers.se (A. Mylonakis), demaz@chalmers.se (C. Demazière), vinai@chalmers.se (P. Vinai).

https://doi.org/10.1016/j.anucene.2022.109300
0306-4549/

the present work, namely FEMFFUSION-TD, FEMFFUSION-FD, CORE SIM+, SIMULATE3/SIMULATE-3 K and QUABOX-CUBBOX. Table 1 shows a comparison of the main characteristics of these codes and the associated methodologies for the modelling of the effect of the neutron noise source.

The codes SIMULATE3/SIMULATE3K and QUABOX-CUBBOX are general nuclear suites for the simulation of a wide variety of dynamic conditions inside an operating nuclear reactor, and they have been adapted to be able to model FA vibrations. Other codes have been developed specifically to simulate the effects of neutron noise sources, namely FEMFFUSION-TD, FEMFFUSION-FD and CORE SIM+.

Some codes use a time-domain integration of the diffusion approximation, varying the cross sections along the transient as FEMFFUSION-TD, SIMULATE-3 K and QUABOX-CUBBOX. Other codes like CORE SIM + and FEMFFUSION-FD rely on a first-order perturbation approximation in the frequency-domain to model the effect of the vibrating assembly. This last methodology has been widely applied in the past to model small oscillating fluctuations in simplified problems (Pázsit, 1977).

The methodologies may differ for the modelling of the neutron noise source. One approach is to introduce the perturbation on the spatial domain where the vibration occurs. On this domain, the perturbation is thus defined as the change of the cross-section compared to its steady-state value. Another approach uses neutron transport codes such as CASMO or SERPENT to re-homogenize the regions according to the different positions of the fuel assembly FA during the vibration. In this way, they build a water gap model that identifies each position of the moving FA with a cross section. Unlike the first approach, the second one is not linear.

The rest of the paper is structured as follows. Section 2 describes the modelling strategy with FEMFFUSION both in the frequency and the time domains and shows some numerical results of this strategy. Then, Section 3 explains how to model FA vibrations with CORE SIM + for three-dimensional reactors. Section 4 and Section 5 are devoted to investigate the strategies that used homogenization through a *water gap model*. In this way, Section 4 investigates the methodology with SIMULATE3/SIMULATE3K and Section 5 studies the methodology with KMACS-ATHLET-QUABOX-CUBBOX. Finally, Section 6 summarizes the main conclusions of the article.

2. Modelling strategy with FEMFFUSION

The modelling strategy developed with the open code FEMFFUSION (Vidal-Ferràndiz et al., 2021) is based on comparing the time-domain methodologies with frequency-domain models of vibrating FA (Vidal-Ferràndiz et al., 2020; Carreño et al., 2022).

2.1. Time domain methodology

One possible approach to simulate transients associated with moving parts inside the reactor core is to use the time dependent neutron diffusion equation, which is an approximation of the neutron transport equation widely used to study the behaviour of nuclear reactors. The neutron diffusion equation assumes that the neutron current is proportional to the gradient of the neutron flux by means of a diffusion coefficient. Although a transport-based solution without spatial homogenization would be required to properly catch the effect of local noise sources, some studies revealed that a diffusion-based solution correctly represents a transport-based solution a few mean free paths away from the noise source and from strong heterogeneities (Yamamoto, 2013).

Particularly, the two energy groups approximation of this equation is considered, assuming that fission neutrons are born in the fast group and there is no up-scattering. This model is of the form

$$\begin{aligned} &\left[v^{-1}\right]\tfrac{\partial \Phi}{\partial t} + \mathscr{L}\Phi = (1-\beta)\mathscr{M}\Phi + \sum_{k=1}^{K}\lambda_k \chi \mathscr{C}_k, \\ &\tfrac{\partial \mathscr{C}_k}{\partial t} = \beta_k\left[\nu\Sigma_{f1}\ \nu\Sigma_{f2}\right]\Phi - \lambda_k \mathscr{C}_k, \quad k = 1,\ldots,K, \end{aligned} \tag{1}$$

where K is the number of delayed neutron precursors groups considered, and the matrices are defined as

$$\left[v^{-1}\right] = \begin{pmatrix} \frac{1}{v_1} & 0 \\ 0 & \frac{1}{v_2} \end{pmatrix},\ \mathscr{L} = \begin{pmatrix} -\vec{\nabla}\left(D_1\vec{\nabla}\right) + \Sigma_{a1} + \Sigma_{12} & 0 \\ -\Sigma_{12} & -\vec{\nabla}D_2\vec{\nabla} + \Sigma_{a2} \end{pmatrix},$$
$$\mathscr{M} = \begin{pmatrix} \nu\Sigma_{f1} & \nu\Sigma_{f2} \\ 0 & 0 \end{pmatrix},\ \Phi = \begin{pmatrix} \phi_1 \\ \phi_2 \end{pmatrix},\ \chi = \begin{pmatrix} 1 \\ 0 \end{pmatrix},$$

where ϕ_1 and ϕ_2 are the fast and thermal neutron fluxes, respectively. The diffusion coefficients, D_g, and the absorption, Σ_{ag}, fission, Σ_{fg}, and scattering cross sections from fast to the thermal group, Σ_{12}, with $g = 1, 2$, depend on the reactor materials, that is, they are position and time dependent functions. The parameter β_k is the yield of delayed neutrons in the k-th precursors group and λ_k is the corresponding decay constant. Both coefficients are related to the delayed neutron precursor decay. Other quantities have their usual notation.

The finite element method (FEM) code, developed at Universitat Politècnica de València (UPV) to solve the time-dependent neutron diffusion equation with vibrating elements, is an option of a more

Table 1
Codes and methodologies used for FA vibrations.

Code	Domain	Neutron Equation	Cross-Section modelling of the noise source	Numerical examples
FEMFFUSION-TD	Time Domain	Diffusion	Volume Averaged	2D FA vibrations
FEMFFUSION-FD	Frequency Domain	Diffusion	Volume Averaged	2D FA vibrations
CORE SIM+	Frequency Domain	Diffusion	Volume Averaged	FA vibrations and Core Barrel vibrations
SIMULATE3/ SIMULATE-3 K (S3K)	Time Domain	Diffusion	Water gap model CASMO-5	FA vibrations and Core barrel vibrations
QUABOX-CUBBOX	Time Domain	Diffusion	Water gap model SCALE	Core barrel vibrations

general neutronic code, FEMFFUSION (Vidal-Ferràndiz et al., 2021), called namely FEMFFUSION-TD. This solver is an open-source C++ neutronic code that solves the multigroup neutron transport equation using the diffusion approximation or the SPN approximation. The code uses the continuous Galerkin finite element method to be able to deal with any type of geometry and any problem dimension (1D, 2D and 3D problems).

2.1.1. Steady-state configuration

For a given transient analysis in a reactor core, usually, a static configuration of the reactor is considered as initial condition. Associated with the time dependent neutron diffusion equation, (1), there is the generalized eigenvalue problem:

$$\mathscr{L}\Phi = \frac{1}{\lambda}\mathscr{M}\Phi, \tag{2}$$

which, in the approximation of two groups of energy without upscattering, is expressed as

$$\begin{pmatrix} -\vec{\nabla}(D_1\vec{\nabla}) + \Sigma_{a1} + \Sigma_{12} & 0 \\ -\Sigma_{12} & -\vec{\nabla}(D_2\vec{\nabla}) + \Sigma_{a2} \end{pmatrix} \begin{pmatrix} \phi_1 \\ \phi_2 \end{pmatrix} = \frac{1}{\lambda} \begin{pmatrix} \nu\Sigma_{f1} & \nu\Sigma_{f2} \\ 0 & 0 \end{pmatrix} \begin{pmatrix} \phi_1 \\ \phi_2 \end{pmatrix}. \tag{3}$$

The fundamental eigenvalue (the largest one) is called the k-effective of the reactor core (k_{eff}). This eigenvalue and its corresponding eigenfunction describe the steady state neutron distribution in the core. In this way, the calculation of the stationary neutron flux distribution is the first step for any transient analysis. To solve the problem defined by (2) a spatial discretization of the equations has to be selected. In this work, a high order Galerkin finite element method is used (Vidal-Ferràndiz et al., 2014; Vidal-Ferràndiz et al., 2020).

2.1.2. Spatial and time discretizations

Once the spatial discretization is performed, the semi-discrete two energy groups time dependent neutron diffusion equation together with the neutron precursors concentration equations are of the form

$$\left[\tilde{\nu}^{-1}\right]\frac{d\Phi}{dt} + L\Phi = (1-\beta_{\text{eff}})M\Phi + \sum_{k=1}^{K}\lambda_k X C_k, \tag{4}$$

$$P\frac{C_k}{dt} = \beta_k(M_{11}\ M_{12})\Phi - \lambda_k P C_k, \quad k = 1,\ldots,K, \tag{5}$$

where L and M are the matrices obtained from the spatial discretization of operators $\mathscr{L}$ and $\mathscr{M}$. Φ and C_k are now the vector of coefficients of the fast and thermal neutron fluxes and the precursors' concentration in terms of the polynomials used in the finite element method. The matrices X and $\left[\tilde{\nu}^{-1}\right]$ are defined as

$$X = \begin{pmatrix} P \\ 0 \end{pmatrix}, \qquad \left[\tilde{\nu}^{-1}\right] = \begin{pmatrix} P\nu_1^{-1} & 0 \\ 0 & P\nu_2^{-1} \end{pmatrix},$$

where the matrix P is the mass matrix of the spatial discretization. For the time discretization of these equations, a first order backward method is used (Vidal-Ferràndiz et al., 2016). Using this method at each time step, a large system of linear equations must be solved:

$$T^{n+1}\Phi^{n+1} = R^n\Phi^n + \sum_{k=1}^{K}\lambda_k e^{-\lambda_k\Delta t_n} X C_k^n, \tag{6}$$

where $\Delta t_n = t_{n+1} - t_n$, the matrices are defined as

$$T^{n+1} = \tfrac{1}{\Delta t_n}\left[\tilde{\nu}^{-1}\right] + L^{n+1} - \hat{a}M^{n+1},$$

$$R^n = \tfrac{1}{\Delta t_n}\left[\tilde{\nu}^{-1}\right] = \tfrac{1}{\Delta t}\begin{pmatrix} P\nu_1^{-1} & 0 \\ 0 & P\nu_2^{-1} \end{pmatrix},$$

and the coefficients are

$$\hat{a} = 1 - \beta_{\text{eff}} + \sum_{k=1}^{K}\beta_k\left(1 - e^{\lambda_k\Delta t_n}\right), \quad \beta_{\text{eff}} = \sum_{k=1}^{K}\beta_k.$$

The preconditioned BICGSTAB method has been chosen to solve these systems, and the preconditioner used has been the incomplete LU preconditioner together with a reordering of the matrix to decrease the fill-in. This system of equations is large and sparse and must be solved for each new time step with a high accuracy (tol $= 10^{-12}$) to be able to distinguish the time dependent neutron noise from the static neutron flux, since the spatial scales of the problem are very different. The mechanical vibration is of the order of few millimetres, and the homogenized fuel assemblies are of the order of tens of centimetres.

The time step Δt_n is maintained constant during all the transient. Small time-steps are usually used to solve the neutron diffusion equation when the term $\left[\tilde{\nu}^{-1}\right]\frac{d\Phi}{dt}$ of Eq. (4) must be accurately represented. However, this term is important only when the neutron flux changes at least one decade over a millisecond. This is not the case of neutron noise analysis calculations. In this way, a time step of $\Delta t = 10^{-2}$ s has been proven to give accurate results. Nevertheless a time step of $\Delta t = 10^{-4}$ s has been used to ensure the convergence of the results. An alternative approach using adaptive method to solve the time dependent neutron diffusion equation is presented in (Carreño et al., 2021).

2.1.3. Fuel assembly vibration simulation in the time-domain

The simulation of the assembly vibration is done by changing in time the homogenized cross-sections of the corresponding materials using a simple volume averaged method. This method for a 1D geometry is schematized in Fig. 1.

The movement of the assembly is taken into account, changing the value of the homogenized cross-sections accordingly to volume-homogenized equations

$$\begin{aligned} \tilde{\Sigma}_{a-1} &= \Sigma_{a-1}, \quad \tilde{\Sigma}_a = \tfrac{1}{L_a}(\Sigma_{a-1}\Delta x + \Sigma_a(L_a - \Delta x)), \\ \tilde{\Sigma}_{a+1} &= \tfrac{1}{L_{a+1}}(\Sigma_a\Delta x + \Sigma_{a+1}(L_{a+1} - \Delta x)). \end{aligned} \tag{7}$$

A similar model is considered for 2D and 3D rectangular geometries. Fig. 2.

Finally, to compare the results obtained from the time-domain analysis with the ones obtained with the frequency-domain methodology, we define the neutron noise in the time-domain as:

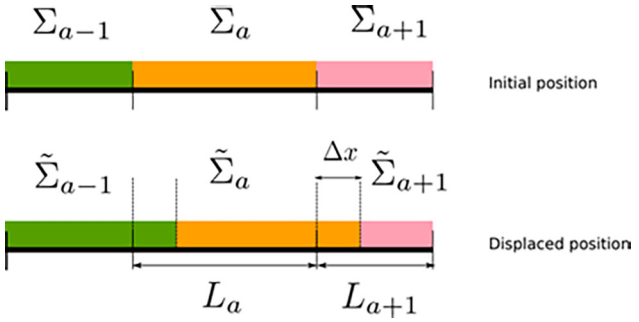

Fig. 1. Schematic disposition for a 1D displacement of a vibrating assembly.

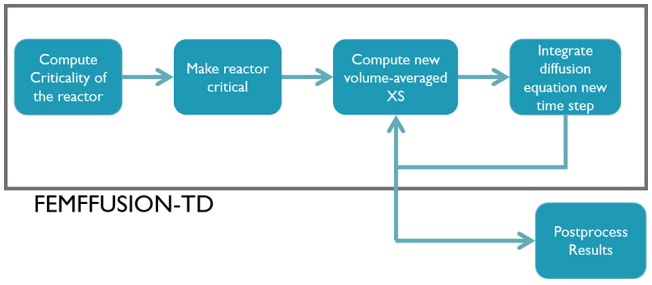

Fig. 2. Scheme of the methodology employed in FEMFFUSION-TD.

$$\delta\phi(r,t) = \phi(r,t) - \phi(r,0). \tag{8}$$

2.2. Frequency domain methodology

The neutron diffusion equation in the frequency-domain has already been successfully used to study other neutron noise sources (Demazière and Andhill, 2005; Demazière, 2006; Demazière and Pázsit, 2009). This section discusses the frequency-domain methodology developed by UPV based on FEMFFUSION and called FEMFFUSION-FD. This tool uses the usual two energy groups diffusion approximation in the frequency-domain in the first-order neutron noise approximation. This code is similar CORE SIM+ (Demazière, 2011; Mylonakis et al., 2021).

The first-order neutron noise theory expresses every time-dependent term $U(t)$ as the sum of its mean value, U_0, and the fluctuation δU around U_0:

$$U(\vec{r},t) = U_0(\vec{r}) + \delta U(\vec{r},t). \tag{9}$$

The fluctuations are assumed to be small compared to the mean values. This allows to neglect second-order terms. Also, the fluctuations of the diffusion coefficients are neglected, so $\delta D_g = 0$ is assumed. Then, a Fourier transform is applied to the neutron diffusion equation. Thus, the first-order neutron noise equation can be written as (Demazière, 2011):

$$-\vec{\nabla}\left(D\vec{\nabla}\delta\phi(\vec{r},\omega)\right) + \Sigma_{\text{dyn}}\delta\phi(\vec{r},\omega) = \delta S(\vec{r},\omega). \tag{10}$$

The perturbation source term $\delta S(\vec{r},\omega)$ is given by the frequency-domain changes in the cross-sections:

$$\delta S(\vec{r},\omega) = \begin{pmatrix}\delta S_1(\vec{r},\omega)\\ \delta S_2(\vec{r},\omega)\end{pmatrix} = [\phi_S]\delta\Sigma_{12} + [\phi_a]\begin{pmatrix}\delta\Sigma_{a1}\\ \delta\Sigma_{a2}\end{pmatrix} + \frac{1}{k_{\text{eff}}}[\phi_f]\begin{pmatrix}\delta\nu\Sigma_{f1}\\ \delta\nu\Sigma_{f2}\end{pmatrix}, \tag{11}$$

where

$$D = \begin{pmatrix}D_1 & 0\\ 0 & D_2\end{pmatrix}, \quad \Sigma_{\text{dyn}} = \begin{pmatrix}-\Sigma_1 & \nu\Sigma_{f2}\left(1-\frac{i\omega\beta_{\text{eff}}}{i\omega+\lambda_{\text{eff}}}\right),\\ \Sigma_{12} & \left(\Sigma_{a2}+\frac{i\omega}{v_2}\right)\end{pmatrix}$$
$$[\phi_s] = \begin{pmatrix}-\phi_1\\ \phi_1\end{pmatrix}, \quad [\phi_a] = \begin{pmatrix}\phi_1 & 0\\ 0 & \phi_2\end{pmatrix}, \quad [\phi_f] = \left(1-\frac{i\omega\beta_{\text{eff}}}{i\omega+\lambda_{\text{eff}}}\right)\begin{pmatrix}\phi_1 & \phi_2\\ 0 & 0\end{pmatrix},$$
$$\Sigma_1 = \Sigma_a + \frac{i\omega}{v_1} + \Sigma_{12} - \nu\Sigma_{f1}\left(1-\frac{i\omega\beta_{\text{eff}}}{i\omega+\lambda_{\text{eff}}}\right). \tag{12}$$

The quantities ϕ_1 and ϕ_2 are the steady state fast and thermal neutron fluxes. The effective constants for the delayed neutron precursor, β_{eff} and λ_{eff}, can be calculated as

$$\beta_{\text{eff}} = \sum_{k=1}^{K}\beta_k, \quad \lambda_{\text{eff}} = \frac{\beta_{\text{eff}}}{\sum_{k=1}^{K}\frac{\beta_k}{\lambda_k}}.$$

The neutron noise equation is a partial differential equation with complex coefficients that has to be solved after the static solution is obtained. The related static eigenvalue problem must be solved with the same spatial discretization as the frequency-domain neutron noise equation to get coherent results. Applying the continuous Galerkin finite element discretization to Eq. (10) leads to an algebraic linear system of equation with the following block structure:

$$\begin{pmatrix}A_{11} & A_{12}\\ A_{21} & A_{22}\end{pmatrix}\begin{pmatrix}\delta\phi_1\\ \delta\phi_2\end{pmatrix} = \begin{pmatrix}\delta S_1\\ \delta S_2\end{pmatrix}, \tag{13}$$

where $\delta\phi_1$ and $\delta\phi_2$ are the algebraic vectors of weights of the noise associated with the fast and thermal neutron fluxes, respectively.

It must be noted that in the time-domain approach a linear system must be solved for each time step, resulting in a large amount of linear systems resolutions for a typical transient, but in the frequency-domain approach only a linear system in the complex domain must be solved. This system is only solved for the specific frequency of the noise source, and this makes this methodology cheaper than the time-domain strategy in terms of the computational cost. The complex linear system is solved with the help of the PETSc library (Balay et al., 2021) using the GMRES solver to obtain $\delta\phi_1$ and $\delta\phi_2$, which are complex quantities.

The results are presented in terms of the fast and thermal neutron noise amplitudes, $|\delta\phi_1|$ and $|\delta\phi_2|$ and the neutron noise phase, $\arg(\delta\phi_1)$ and $\arg(\delta\phi_2)$, corresponding to the argument of the complex number in the $[-180°, 180°]$ interval. Sometimes, it is convenient to represent the relative neutron noise amplitude defined as

$$|\delta\phi_1|_{\text{REL}} = \frac{|\delta\phi_1|}{\phi_1}, \quad |\delta\phi_2|_{\text{REL}} = \frac{|\delta\phi_2|}{\phi_2},$$

where ϕ_1 and ϕ_2 are the steady-state fast and thermal neutron fluxes, respectively, previously solved using the same spatial discretization.

2.2.1. Fuel assembly vibration simulation in the frequency-domain

There are different models to describe the vibration of a FA in the frequency-domain. In frequency domain codes, we have used the ε/D model, in which the vibration is converted into a spatially localized cross-section perturbation (Pázsit, 1977; Pázsit and Demazière, 2010).

Assuming a nodal representation of the system (i.e. each FA is replaced by homogenized regions), one oscillating FA can be modelled as two moving interfaces between homogeneous materials. For the sake of illustration, we consider hereafter two adjacent homogeneous regions and the corresponding possible displacement of the boundary between those regions, as shown in Fig. 3.

The cross section Σ_α, near the interface $x = b$ between two material regions, can be described as

$$\Sigma_\alpha(x) = (1 - \mathscr{H}(x-b))\Sigma_\alpha^I + \mathscr{H}(x-b)\Sigma_\alpha^{II}, \tag{14}$$

where $\mathscr{H}$ is the unit step function, Σ_α^I and Σ_α^{II} are the cross sections at region *I* and *II*, respectively.

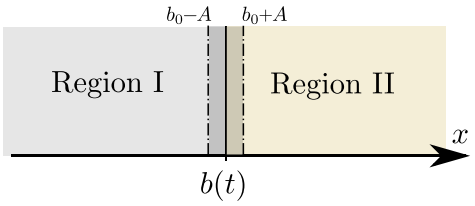

Fig. 3. Vibrating interface between two regions.

A moving interface as $b(t) = b_0 + A\sin(\omega_p t)$, results in

$$\Sigma_\alpha(x,t) = (1 - \mathscr{H}(x - b_0 - A\sin(\omega_p t)))\Sigma_\alpha^I + \mathscr{H}(x - b_0 - A\sin(\omega_p t))\Sigma_\alpha^{II}. \quad (15)$$

Using the first order Taylor expansion around $x - b_0$, the cross-section perturbation can be expressed as:

$$\delta\Sigma_\alpha(x,t) = \left(\Sigma_\alpha^I - \Sigma_\alpha^{II}\right) A\sin(\omega_p t)\delta(x - b_0), \quad (16)$$

and, in the frequency-domain, the perturbation can be written as follows:

$$\delta\Sigma_\alpha(x,\omega) = -i\pi A\left(\Sigma_\alpha^I - \Sigma_\alpha^{II}\right)\delta(x - b_0)\left(\delta(\omega - \omega_p) + \delta(\omega + \omega_p)\right). \quad (17)$$

If the perturbation is introduced node-wise, one could assume that the perturbed region is $x \in [b_0 - A, b_0 + A]$ at angular frequency ω_p, with an average value of $\delta\Sigma_\alpha = -\frac{1}{2}i\pi\left(\Sigma_\alpha^I - \Sigma_\alpha^{II}\right)$ in the perturbed region. If the spatial mesh used does not match the perturbed region, the perturbation must be scaled accordingly. In (Rouchon, 2016), we can find the full analytical expression for the model of a vibrating FA in the frequency-domain. This model highlights the fact that a monochromatic displacement introduces polychromatic perturbations of the homogenized cross-sections on which the boundary is moving. This is due to the fact that those homogenized regions are perturbed only during parts of the vibration period.

To test the accuracy of the first order approximation, a numerical Fast Fourier transform (FFT) of a time-dependent cross section $\Sigma_\alpha(x,t)$ is calculated. The numerical FFT was obtained for a one-dimensional moving interface perturbation with $\Sigma_\alpha^I - \Sigma_\alpha^{II} = 1$ and a frequency of 1 Hz.

Fig. 4 shows the spectrum of the perturbation at different spatial points using the FFT. The amplitude of the cross-section perturbation is maximum at 1 Hz, and the amplitudes at other frequencies are smaller. This Figure also shows the absolute value of the amplitude of the perturbation, $|\delta\Sigma_\alpha|$, at 1 Hz for the numerical FFT and the first order approximation. The first order approximation has the same perturbation integral as the FFT, and it can be introduced using only one node.

The higher harmonics corresponding to frequencies of 2 Hz, 3 Hz and 4 Hz are usually not taken into account in frequency-domain codes. These higher harmonics require additional calculations, as the frequency-domain codes solve one frequency each time. Here, we study the contributions of those higher harmonics by solving the time-dependent problem with FEMFFUSION. In this way, the time-domain approach does not decompose the perturbation and does not require any assumption in the perturbation source. In (Rouchon, 2016), more results corresponding to the higher harmonics of the noise source are given.

2.3. Numerical results

2.3.1. Two-dimensional BIBLIS benchmark

The BIBLIS 2D benchmark is selected to compare the frequency and time-domain analysis for a vibrating FA. This is a classical two-group neutron diffusion problem taken as a benchmark for different numerical codes. The material and geometry definition of the benchmark can be found in (Hébert, 1985). The problem is made critical before starting the time-dependent calculation by dividing $\nu\Sigma_{fg}$ by k_{eff}.

The assembly in the position (6,6) is selected to be oscillating along the x direction as

$$x_i(t) = x_{i0} + A\sin(\omega_p t),$$

where $x_i(t)$ represents each position of the vibrating assembly in one oscillation, originally placed at x_{i0}. The selected amplitude of the movement is $A = 1$ mm and the frequency of the vibration is 1 Hz, i.e. $\omega_p = 2\pi$. The perturbation for the time-domain calculation is inserted by changing the cross sections at each time step and modelling the movement of the FA by volume-averaged cross sections. For the frequency-domain calculation, the perturbation is inserted according to the first order approximation as explained in Section 2.2.1. In this way, the perturbation is inserted cell wise in the adjacent cells next to the moving FA as shown in Fig. 5.

The value of the cross sections and the perturbed cross sections are given in (Vidal-Ferràndiz et al., 2020) following the formula, $\delta\Sigma_\alpha = -i\frac{\pi}{2}\left(\Sigma_\alpha^I - \Sigma_\alpha^{II}\right)$. Two perturbed regions are then defined: one on the left and one on the right, respectively, of the moving boundary of the vibrating FA. These regions have the same cross-section perturbation amplitude but a phase lag of 180°.

Due to the different scales of the problem, a fine mesh needs to be used to accurately solve the problem. In the time-domain analysis, a refined spatial mesh in the surroundings of the moving FA

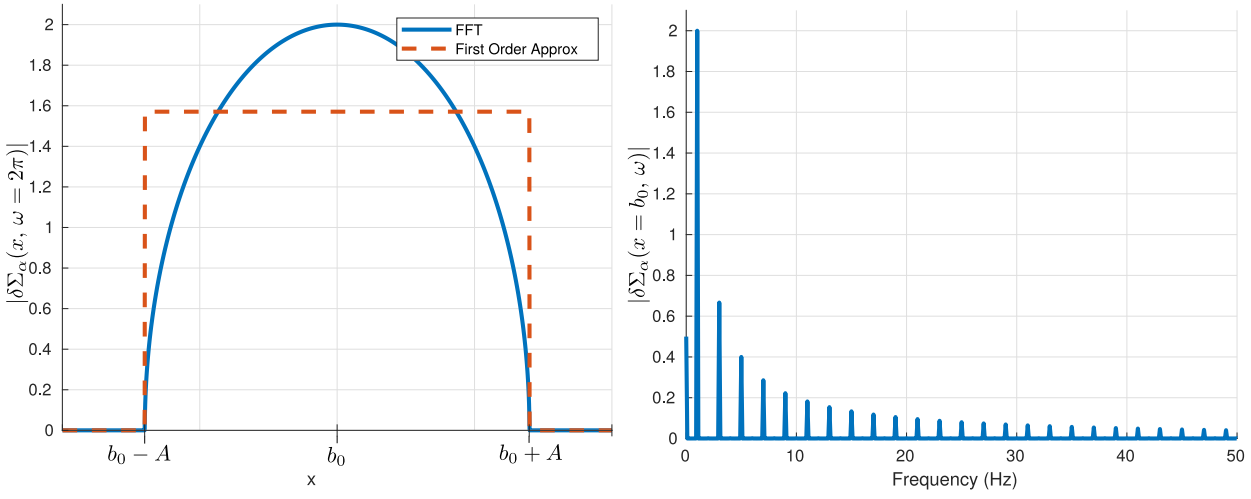

(a) Cross section perturbation amplitude at 1 Hz.

(b) Spectrum at b_0.

Fig. 4. Amplitude and spectrum of the numerical FFT at different spatial points.

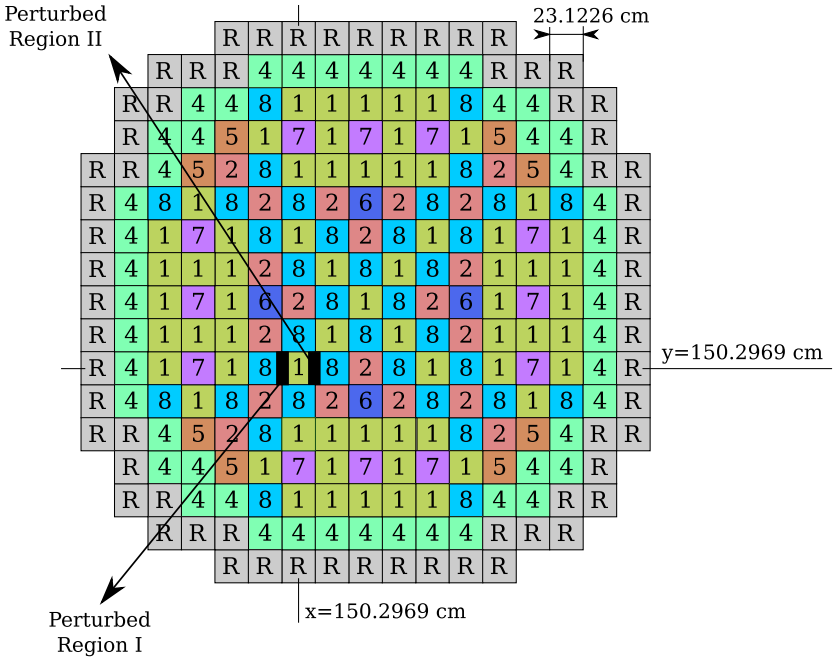

Fig. 5. Materials and perturbed regions of the 2D BIBLIS reactor.

with 869 cells and cubic polynomials in the FEM are used. In the frequency-domain analysis, a uniform mesh of 4624 cells is employed. If these fine meshes were not used, the effect of the FA vibration could be overestimated (Vidal-Ferràndiz et al., 2020).

Fig. 6 shows the spatial distribution of the amplitude of the relative neutron noise in the frequency-domain, calculated with the time-dependent code FEMFFUSION-TD at 1 Hz. In this figure, the relative neutron noise is represented in percentage of the steady-state neutron flux. It can be seen that the induced fast neutron noise has an influence on larger scales through the reactor compared to the thermal noise, due to the larger mean free path of fast neutrons. On the other hand, the thermal noise is localized in the surroundings of the oscillating FA. Two clear peaks can be observed in these figures at the position of the moving interfaces, where the cross sections change along the FA movement.

When a small perturbation in a critical model without thermal–hydraulic feedback is introduced (even a sinusoidal perturbation), mathematically the system becomes unstable, since k_{eff} deviates from unity. Nevertheless, in a real reactor, this change in criticality is small and will be attenuated by the thermal–hydraulic feedback that has a stabilizing effect or the reactivity control system of the nuclear plant. In this case, the maximum change in reactivity is only $\rho = (k_{\text{eff}} - 1)/k_{\text{eff}} \approx 1.5 \times 10^{-8}$. Nevertheless, it is possible to introduce some kind of average kinetic eigenvalue to mitigate this effect (Gammicchia et al., 2020). This correction was not implemented in this work because of the smallness of the perturbation in reactivity. If the simulation were longer or the perturbation greater, this kind of treatment would be necessary.

Fig. 7 shows a comparison of the relative amplitude and the phase of neutron flux noise for the thermal group along

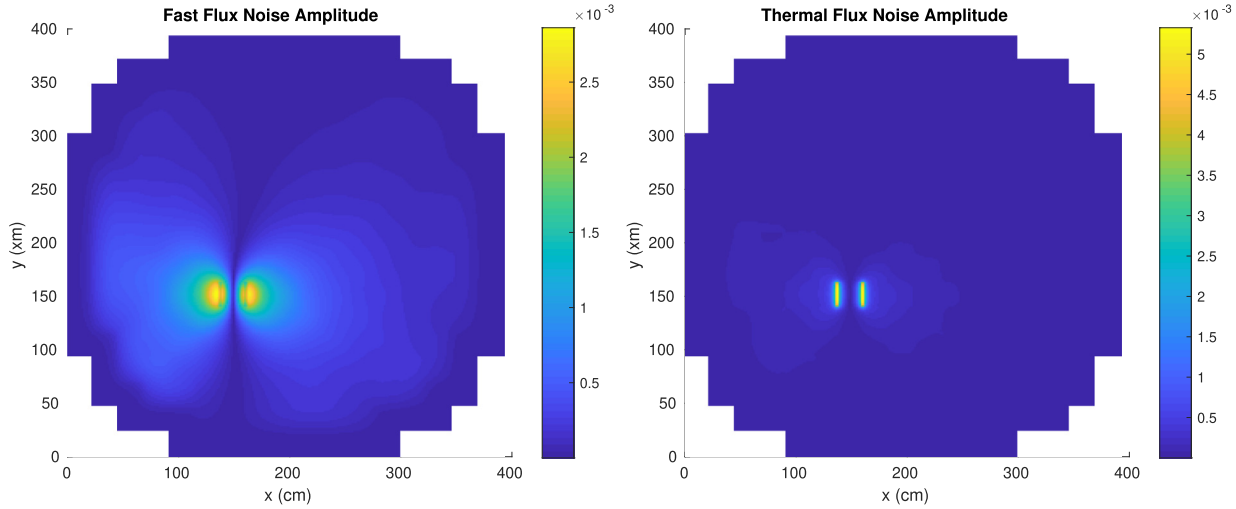

Fig. 6. Noise amplitudes for the 2D BIBLIS reactor at 1 Hz.

$y = 150.2969$ cm, obtained with the FEMFFUSION-TD code and the CORE SIM + code, in other words, between the time-domain and the frequency-domain approaches. A close agreement is observed for both the amplitude and the phase of the neutron noise for the vibration frequency at 1 Hz, especially far from the FA vibration. We can observe that the vibrating FA produces a phase change from 90° to −90° in the induced noise. This Figure demonstrates that a time step $\Delta t = 10^{-2}$ s is small enough to accurately reproduce the noise amplitude results. Similar results are obtained if the noise associated with the fast flux are compared.

The difference between the frequency-domain and the time-domain approaches are small in regions far away from the perturbation, although the relative differences at the perturbation location are comparably bigger. This difference is mainly caused by the spatial discretization error. The FEM approach is known to better capture steep gradients, as is the case close to the noise source.

Fig. 8 shows the thermal neutron noise magnitudes for three different oscillation amplitudes and three different frequencies calculated with FEMFFUSION-TD. Fig. 8a displays the neutron noise amplitude associated with the thermal flux for different vibrations amplitudes at the neutron detector, situated at $(x = 104.0517, y = 150.2969)$ cm. These results are calculated with FEMFFUSION-TD. In these Figures, a proportional dependency of the neutron noise magnitude with the amplitude of the FA vibration amplitude can be observed. Fig. 8b shows the fast and the thermal neutron noise magnitudes for three different oscillation frequencies (0.02 Hz, 1 Hz and 50 Hz) computed with FEMFFUSION-TD. Even though the 0.02 Hz and 50 Hz frequencies are not realistic values for mechanical vibrations of FA, they cover a wider range of possible frequencies to complete the analysis.

2.3.2. Three-dimensional hexagonal VVER-1000 benchmark

As a case of study for a hexagonal reactor, a typical hexagonal VVER-1000 reactor core is considered (Malmir and Vosoughi, 2015). This benchmark has a 1/12 reflective symmetry but, as the inserted perturbation is not symmetrical, the whole reactor must be modelled. The core is composed of 163 fuel assemblies surrounded by 54 reflector cells. Fig. 9 shows the materials layout of the core. The FA pitch is 23.6 cm, and the active height is 355 cm. Therefore, the total height is 426 cm, including 35.5 cm thick reflectors in the upper and the lower part of the core. The reactor is discretized into 24 planes, each one of them of 17.75 cm thick.

A generic absorber of variable strength is inserted in the FA marked with a cross (×) in Fig. 9, on the plane 12. Such a noise source corresponds to a 10% perturbation of the cross sections Σ_{a1} and Σ_{a2}.

Table 2 shows the convergence of the solution depending on the methodology employed, and the polynomial degree used in the FEM shape functions, the Finite Element Degree (FED). To compare the solutions, we have defined the following error indicators:

$$\zeta_g = 100 \times \frac{1}{N_c} \sum_{c=1}^{N_c} \frac{||\delta\bar{\phi}_{c,g}| - |\delta\bar{\phi}^*_{c,g}||}{|\delta\bar{\phi}^*_{c,g}|} \ \%, \quad g = 1, 2, \tag{18}$$

$$\eta_g = 100 \times \frac{1}{N_c} \sum_{c=1}^{N_c} \frac{|\arg\left(\delta\bar{\phi}_{c,g}\right) - \arg\left(\delta\bar{\phi}^*_{c,g}\right)|}{|\arg\left(\delta\bar{\phi}^*_{c,g}\right)|} \ \%, \quad g = 1, 2, \tag{19}$$

where the values with $*$ represent the reference results that are extracted with a very accurate time-domain calculation obtained with FED = 5 and $\Delta t = 10^{-4}$s. The quantity $\delta\bar{\phi}_{c,g}$ is the average neutron noise at the hexagonal cell c. The parameter N_c is the number of hexagonal cells in the reactor.

Fig. 10 presents the relative noise magnitude for both the fast and the thermal fluxes. Fig. 11 displays the neutron noise phase obtained with FED = 3 and with the frequency-domain approach. The results show that the thermal neutron noise is mostly localized, while the fast neutron noise has influence over a wider region. Also, for this perturbation, the phase of the neutron noise is similar throughout the entire reactor. Table 2 shows the neutron noise results comparison for the frequency-domain and time-domain methodologies employed and the FED ranging from 1 to 3. This Table shows that the differences between the frequency-domain and time-domain methodologies using the same FED are small, validating both methodologies. It also indicates that calculations with linear shape functions do not provide accurate enough results.

These results verify both the frequency-domain methodology and the time-domain methodology against a generic absorber of variable strength in a selected location in a three-dimensional hexagonal reactor.

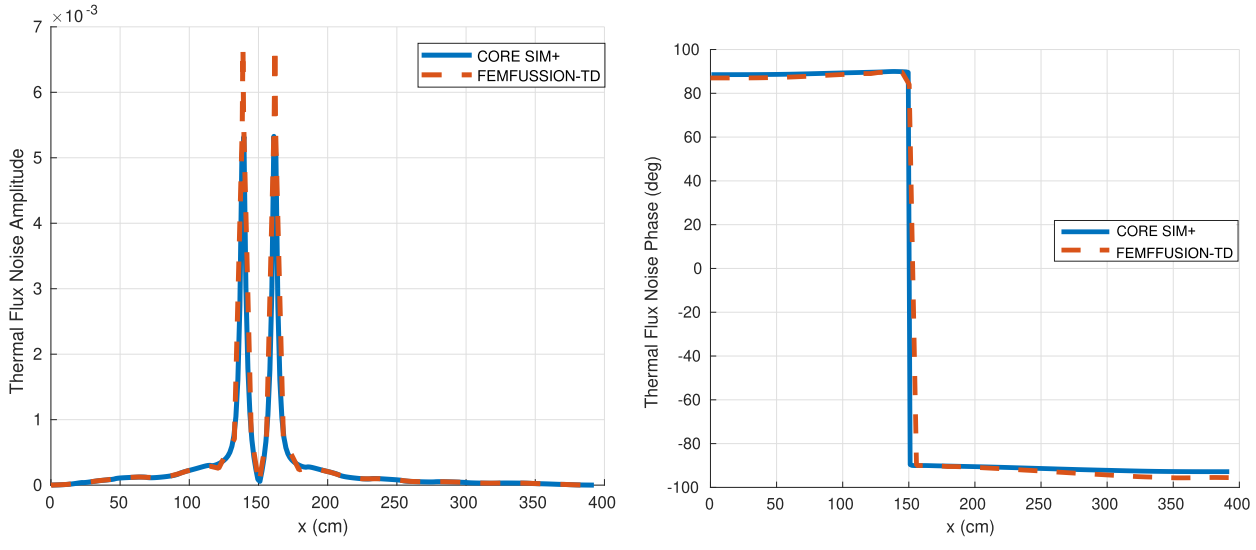

(a) Noise amplitude.

(b) Noise Phase.

Fig. 7. Relative thermal noise for 2D BIBLIS reactor in $y = 150.2969$ cm at 1 Hz.

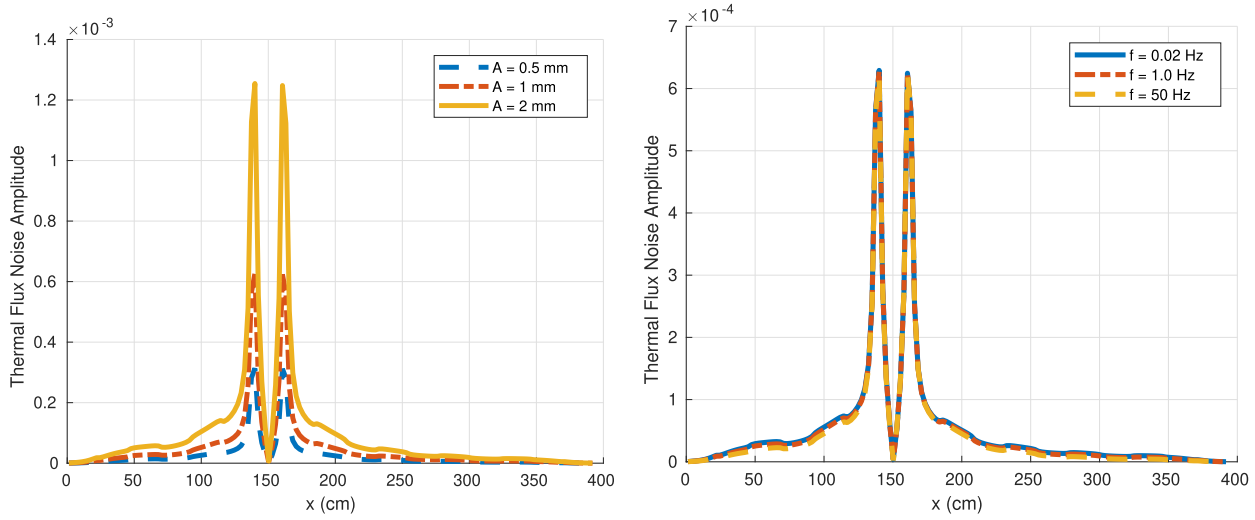

(a) Thermal flux noise. (b) Thermal flux noise.

Fig. 8. Noise magnitude comparison for different amplitudes and frequencies of vibrations in the 2D BIBLIS reactor at $y = 150.2969$ cm computed with FEMFFUSION-TD.

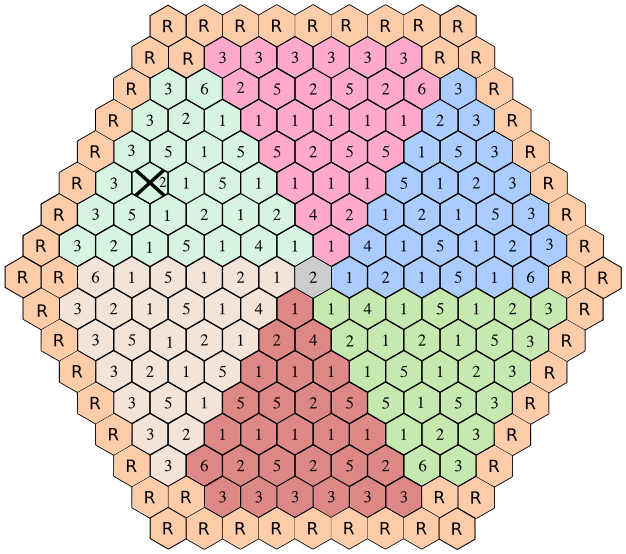

Fig. 9. Material layout of the VVER-1000 benchmark.

3. Modelling strategy with CORE SIM+

The computational tool CORE SIM + is developed to model the reactor transfer function and simulate scenarios induced by neutron noise sources such as mechanical vibrations of fuel assemblies and of the core barrel (Mylonakis et al., 2021). The simulator relies on the previous experience of CORE SIM (Demazière, 2011) and its new improved numerical scheme allows a more accurate modelling of neutron noise problems and more efficient numerical performances. Such a scheme can make use of uniform or non-uniform meshes for the spatial discretization of the neutron balance equations, and acceleration techniques and preconditioning for increasing the convergence rate of the solution.

3.1. Governing equations

The tool CORE SIM + is based on a two-energy group diffusion model. The calculation scheme first requires the solution of the criticality problem associated with the system under study. After the critical neutron flux is determined, the neutron noise is obtained from the dynamic equations in the frequency domain. For the calculation of the critical neutron flux ϕ in a nuclear reactor, CORE SIM + uses the 3-dimensional, 2-energy group neutron diffusion equations:

$$\left\{\nabla\cdot\begin{bmatrix}D_1 & 0\\ 0 & D_2\end{bmatrix}\nabla+\begin{bmatrix}-\Sigma_{a1}-\Sigma_{12} & 0\\ \Sigma_{12} & -\Sigma_{a2}\end{bmatrix}\right\}\times\begin{bmatrix}\phi_1\\ \phi_2\end{bmatrix} = \frac{1}{k_{\text{eff}}}\begin{bmatrix}-\nu\Sigma_{f1} & -\nu\Sigma_{f2}\\ 0 & 0\end{bmatrix}\times\begin{bmatrix}\phi_1\\ \phi_2\end{bmatrix}. \tag{20}$$

Considering a neutron noise source in the critical system, the induced neutron noise $\delta\phi$ is evaluated with the following dynamic equations in the frequency domain:

$$\left\{\nabla\cdot\begin{bmatrix}D_1 & 0\\ 0 & D_2\end{bmatrix}\nabla+\Sigma_{dyn}^{crit}\right\}\times\begin{bmatrix}\delta\phi_1\\ \delta\phi_2\end{bmatrix} = \begin{bmatrix}\delta S_1\\ \delta S_2\end{bmatrix}. \tag{21}$$

Table 2
Convergence table for the noise of 3D VVER-1000 reactor.

Methodology	FED	ζ_1 (%)	ζ_2 (%)	η_1 (%)	η_2 (%)
Frequency-domain	1	10.51	10.58	0.03	0.03
Frequency-domain	2	1.58	1.58	0.04	0.04
Frequency-domain	3	0.42	0.42	0.04	0.04
Time-domain	1	11.63	11.70	0.02	0.02
Time-domain	2	1.23	1.25	0.00	0.00
Time-domain	3	0.19	0.20	0.00	0.00

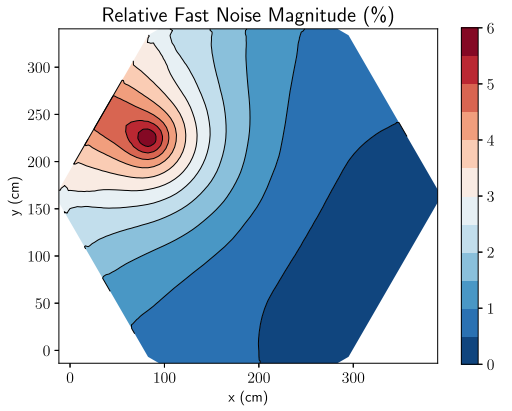

(a) Relative fast flux noise.

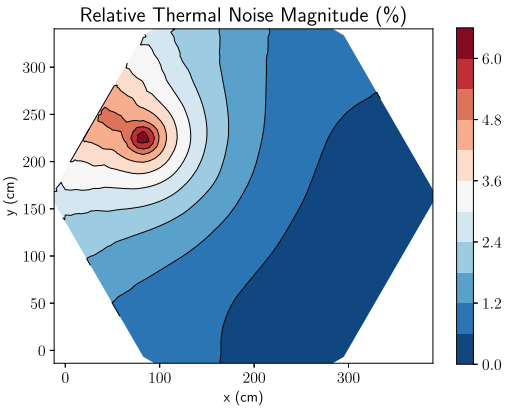

(b) Relative thermal flux noise.

Fig. 10. Relative noise amplitudes at the 3D VVER 1000 reactor.

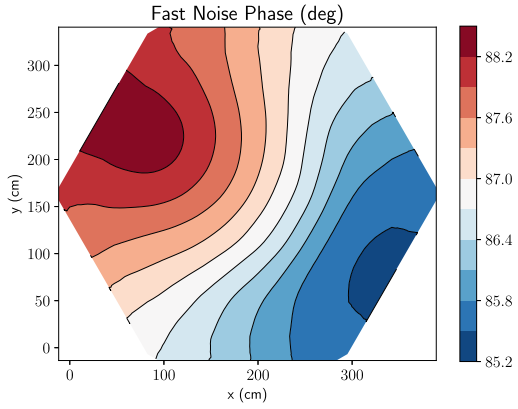

(a) Fast flux phase.

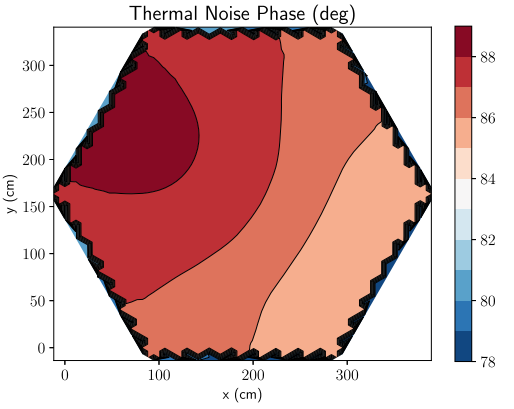

(b) Thermal flux phase.

Fig. 11. Noise phase at the mid-plane of 3D VVER 1000 reactor.

The neutron noise source on the right-hand side of Eq. (21) is modelled as small fluctuations of the macroscopic cross sections, i.e.

$$\begin{pmatrix}\delta S_1\\ \delta S_2\end{pmatrix} = [\phi_S]\delta\Sigma_{12} + [\phi_a]\begin{pmatrix}\delta\Sigma_{a1}\\ \delta\Sigma_{a2}\end{pmatrix} + \frac{1}{k_{\text{eff}}}[\phi_f]\begin{pmatrix}\delta\nu\Sigma_{f1}\\ \delta\nu\Sigma_{f2}\end{pmatrix}, \tag{22}$$

The notation used in Eqs. (20)–(22) is defined in Eq. (12), more details of it can be found in, e.g., (Mylonakis et al., 2021). These equations are similar to the equations studied in Section 2.2.

3.2. Numerical methods

The physical system is discretized using a rectilinear grid that is selected before the calculation and is kept fixed for all the analysis. The choice of a rectilinear grid allows the generation of non-uniform meshes. Thus, it has the advantage that a finer resolution can be specified for regions where perturbations are very localized and the gradient of the neutron flux is strong, while coarser cells are used for those regions where the spatial variation of the system properties and of the neutron flux is less remarkable. Accordingly, computational effort is saved without compromising the accuracy. The spatial discretization scheme is such that Marshak or reflective Boundary Conditions (BCs) can be used.

After the spatial discretization of the equations, the static problem of Eq. (20) and the neutron noise problem of Eqs. 21,22 can be respectively rewritten in matrix form as:

$$\mathbf{A}_{\text{crit}}\Phi_{\text{crit}} = \frac{1}{k_{\text{eff}}}\mathbf{F}\Phi_{\text{crit}}, \tag{23}$$

$$\mathbf{A}_{\text{noise}}\delta\Phi_{\text{noise}} = \mathbf{S}_{\text{noise}}, \tag{24}$$

In Eqs. 23,24, the coefficient matrices are large, sparse and banded, and their size is $2N \times 2N$ since the number of nodes of the spatial grid is N and the neutron energy groups are 2. The matrices are constructed using the coordinate format. This format stores the diagonals in three vector-arrays of known length: one containing the values of the non-zero entries, one integer array containing their row indices and another integer array containing their column indices. When all diagonals have been computed, the matrix is assembled and stored in a compressed sparse matrix format. Following this strategy, one operates on vector-arrays of known length during the construction phase, avoiding any dynamic allocation of a compressed sparse matrix that would reduce the speed of the process.

Numerical methods suitable for a flexible neutron noise simulator that allow fast convergence rates were investigated and discussed in (Mylonakis et al., 2020). Here, the methods used in CORE SIM + are summarized.

The steady-state system given in Eq. (23) is an eigenvalue problem and three options are available in CORE SIM + for their solution. The first method is the standard non-accelerated Power Method (PM). The second option is PM accelerated with Chebyshev polynomials (Ferguson and Derstine, 1977). The third alternative is PM combined with a nonlinear acceleration based on the Jacobian Free Newton Krylov (JFNK) algorithm, as proposed by (Gill and Asmy, 2009). In reactor static calculations, Mylonakis et al. (2020) showed that the JFNK-accelerated PM can meet tight convergence criteria, which are not always feasible for the Chebyshev accelerated PM.

Linear systems are generated from each iteration of PM when solving the eigenvalue problems. In addition, the neutron noise problem represents a fixed source problem, which requires the solution of the linear system given in Eq. (24). As linear solver, CORE SIM + applies the iterative Generalized Minimal RESidual (GMRES) method. The acceleration of the convergence is obtained from a preconditioner, that can be chosen between the Symmetric Gauss–Seidel (SGS) preconditioner and the Incomplete LU with zero fill-in - ILU(0) preconditioner. Externally constructed preconditioners can also be provided as inputs to the solver.

3.3. Modelling of neutron noise sources

The tool CORE SIM + allows the simulation of neutron noise induced by different types of perturbations. These perturbations are described in terms of fluctuations of macroscopic neutron cross sections according to Eq. (22) and can reproduce absorbers of variable strength, vibrations of fuel assemblies, vibrations of the core barrel, vibrations of control rods, and perturbations that are transported by the coolant flow along the axial direction of the core. A detailed discussion on the modelling of these noise sources can be found in (Demazière and Dokhane, 2019).

3.4. Calculation of neutron noise

Once the model of the source term has been built, two different strategies for the calculation of the neutron noise are implemented in CORE SIM+. The first strategy is to provide the model of the neutron noise source to Eq. (21) via Eq. (22) and then calculate the neutron noise directly from Eq. (21). The second strategy is to first determine the Green's functions $G_{g\to g'}(\mathbf{r},\mathbf{r}',\omega)$ by solving Eq. (21) where the source term for the energy group g is replaced with the Dirac delta function and the source term for the other energy group is equal to zero. Then the neutron noise is evaluated from the convolution of the Green's function and the noise source, i.e.

$$\begin{bmatrix}\delta\phi_1\\ \delta\phi_2\end{bmatrix}=\begin{bmatrix}\int_V [G_{1\to1}(\mathbf{r},\mathbf{r}',\omega)\delta S_1(\mathbf{r}',\omega)+G_{2\to1}(\mathbf{r},\mathbf{r}',\omega)\delta S_2(\mathbf{r}',\omega)]d^3\mathbf{r}'\\ \int_V [G_{1\to2}(\mathbf{r},\mathbf{r}',\omega)\delta S_1(\mathbf{r}',\omega)+G_{2\to2}(\mathbf{r},\mathbf{r}',\omega)\delta S_2(\mathbf{r}',\omega)]d^3\mathbf{r}'\end{bmatrix}. \tag{25}$$

The advantage of the second method is that the Green's function is calculated just only once, and then it can be used to reconstruct the neutron noise induced by any perturbation.

3.5. Simulation of neutron noise induced by vibrations in the core

The vibrations of core components are among the most relevant neutron noise sources in a nuclear reactor. Therefore, two hypothetical scenarios are hereafter analysed with CORE SIM+, in which a vibration of a FA and a pendular vibration of the core barrel are respectively prescribed in a PWR. For these simulations, the system configuration is a MOX/UO2 core of a four-loop Westinghouse PWR, see (Kozlowski and Downar, 2003).

3.5.1. Fuel assembly vibration

The vibration of a FA is modelled using the so-called ϵ/d approximation (Pázsit, 1977). Accordingly, the macroscopic cross sections are perturbed with δ-functions at the interfaces between the vibrating FA and the surrounding regions. The schematic in Fig. 12 shows a one-dimensional configuration with three homogenized fuel assemblies, of which the FA II vibrates in the x-direction. In this case, the fluctuation of the generic cross section $\Sigma_{\alpha,g}$ in the frequency domain is given as:

$$\begin{aligned}\delta\Sigma_{\alpha,g}(x,z,\omega)=&\,h(z)\epsilon_x(\omega)\delta(x-a_0)\left[\Sigma_{\alpha,g,I}-\Sigma_{\alpha,g,II}\right]\\&+h(z)\epsilon_x(\omega)\delta(x-b_0)\left[\Sigma_{\alpha,g,II}-\Sigma_{\alpha,g,III}\right].\end{aligned} \tag{26}$$

The quantity $\epsilon_x(\omega)$ is the displacement of the vibrating FA along x, $h(z)$ is the axial shape of the perturbation, a_0 is the equilibrium position of the boundary between the fuel assemblies I and II, and b_0 is the equilibrium position of the boundary between the fuel assemblies II and III. Eq. (26) is introduced in Eq. (22) so that the proper noise source is built for the evaluation of the neutron noise. Eq. (26) is similar to Eq. (17) but it takes into account the possibility of different axial shapes $h(z)$ of the mechanical vibration.

Fuel assemblies in a nuclear reactor may vibrate according to different patterns and modes. A FA vibration supported on both sides and for its second vibration mode is considered hereafter. For this case, the axial shape $h(z)$ in Eq. (26) is given by the following expression:

$$h(z)=A\sin(k_v z). \tag{27}$$

The parameter k_v is equal to $2\pi/H$, with H being the height of the reactor.

Fig. 13 shows the radial distribution of the computed neutron noise at elevation $z=234.32$ cm in the reactor core when oscillating the FA located at radial position $x=y=74.97$ cm, in the North-East quadrant, with a frequency of 7 Hz. As expected, the highest relative amplitude is found in the vicinity of the vibrating FA (Fig. 13a-b). The solver also predicts an out-of-phase behaviour of the noise between the left and the right sides of the vibrating FA (Fig. 13c-d). Such a feature is typical of the perturbation (e.g., Verma et al., 2019), although not systematically present, depending on the noise source position, system configuration and system size. Fig. 14 gives the axial distribution of the thermal neutron noise calculated for the FA in the centre of the core. The relative amplitude has a minimum at mid-elevation (Fig. 14a), and the noise in the upper and lower parts of the FA is out of phase (Fig. 14b). This behaviour is consistent with the prescribed axial shape of the noise source (Fig. 14c-d).

3.5.2. Core barrel pendular vibration

The vibration of the core barrel may occur according to different modes. For the sake of illustration, only the pendular mode of the core barrel vibration is considered hereafter. It consists of a relative oscillation of the active fuel core with respect to the reflector, so it is equivalent to a collective movement of all the fuel assemblies. This type of core barrel vibration is modelled by introducing a perturbation at the boundary between the active core and reflector regions. The perturbations for all the outer fuel assemblies are computed with Eq. (26). The second term on the right-hand side of Eq. (26) is zero for the fuel assemblies with the left boundary

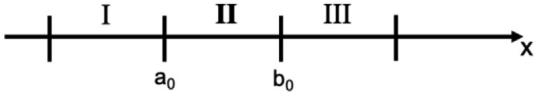

Fig. 12. Schematic of 3 fuel assemblies, with FA II vibrating in the x-direction and FA I and III being fixed.

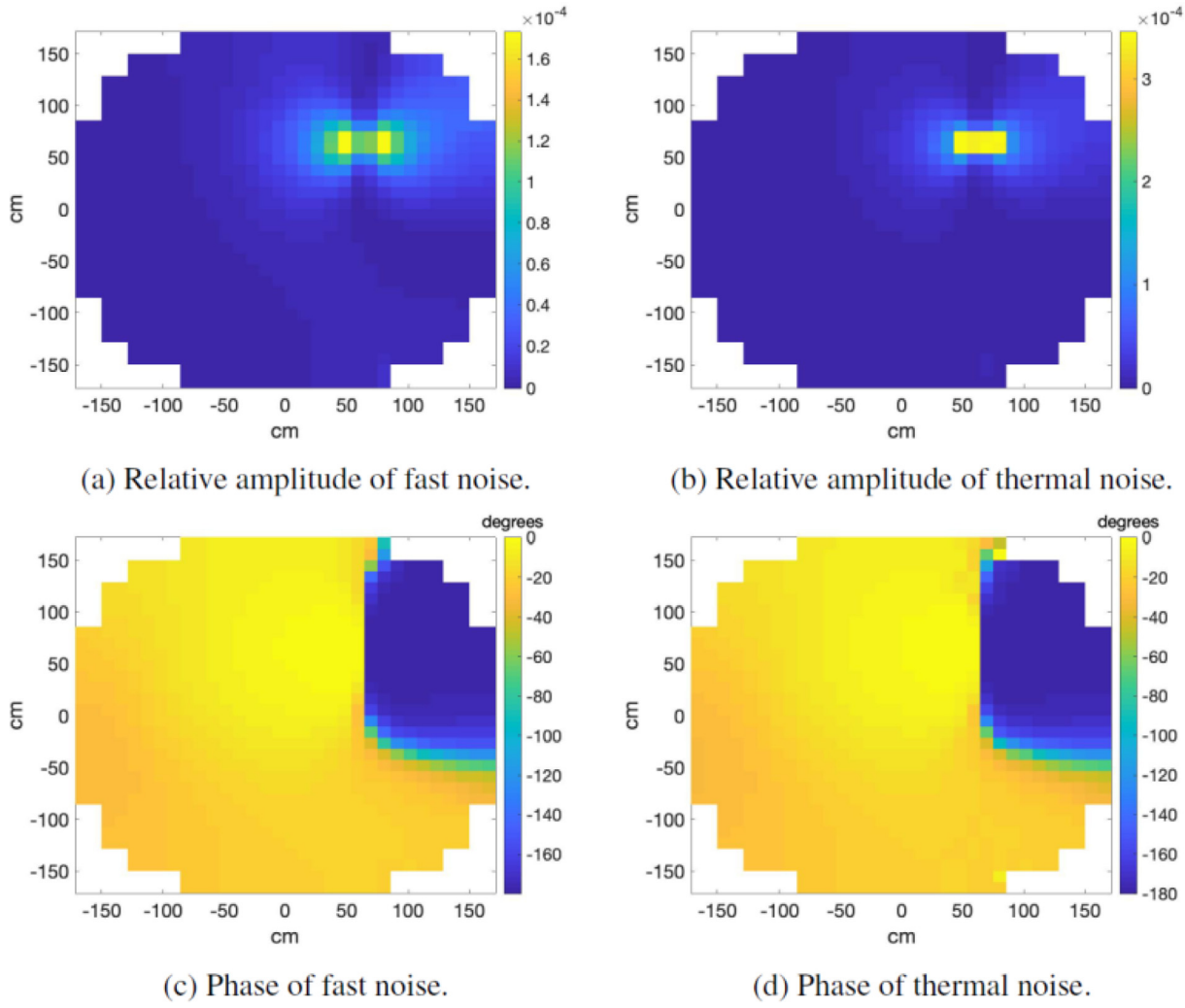

Fig. 13. Radial distribution of the computed neutron noise induced by the vibration of a FA, at axial elevation $z = 234.32$ cm.

next to the reflector, whereas the first term is zero for the fuel assemblies with the right boundary next to the reflector.

In this simulation, the frequency of the vibration is assumed to be 7 Hz. Fig. 15 shows the computed neutron noise radial distribution at mid-elevation of the reactor core. As expected, the amplitude is higher around the interface between the fuel region and the reflector, i.e., the location of the noise source. The noise amplitude is zero in the middle of the reactor, along the line perpendicular to the direction of vibration, because of the symmetry of the problem. The simulation predicts well the out-of-phase behaviour between the two halves of the core, which is typical of the perturbation. The fast and thermal components of the noise have opposite phases; such a relationship is determined by the respective weight and sign of the fast and thermal noise sources (Eq. (22)) via the coupled fast and thermal noise equations (Eq. (21)).

4. Modelling strategy with CASMO-5, SIMULATE-3 and SIMULATE-3 K

The Studsvik Scandpower (SSP) developed codes as CASMO-5, SIMULATE-3, and SIMULATE-3 K (S3K) (Ferrer, 2015; Cronin et al., 1995; Grandi, 2011) that are commercially available advanced simulation tools. These tools were adapted to be used as a basis for numerical noise analysis. In this study, the tools are used to model a certain type of mechanically vibrating noise source, i.e., FA vibrations, and study their impact on the neutron noise phenomenology. An illustration of the sequence of the codes is shown in Fig. 16.

4.1. Model

In this approach, FA vibration is assumed to be a stationary process. The noise source is modelled in terms of fluctuations of two group assembly-wise homogenized macroscopic cross sections. This modelling approach is based on the principle that a vibrating FA leads to time-dependent modification of the water-gap thickness surrounding the FA in the direction of motion, which is reflected in the perturbed cross sections. A detailed description of the modelling steps involving the various simulations codes, the delta-gap model, the assembly vibration model and the supplementary MATLAB procedures is given below.

In the first step of modelling the neutron noise source, CASMO-5 is employed to generate the two-group homogenized macroscopic cross sections taking into account the vibrating fuel assemblies via the varying water-gap widths using the ‘delta-gap model’. To that effect, an additional delta gap branch calculation is performed on top of the default standard case matrix. The delta gap model assumes that the lateral vibration of a FA can be represented as modification of the water-gaps surrounding the moving FA, instead of modelling physically oscillating fuel pins, and by

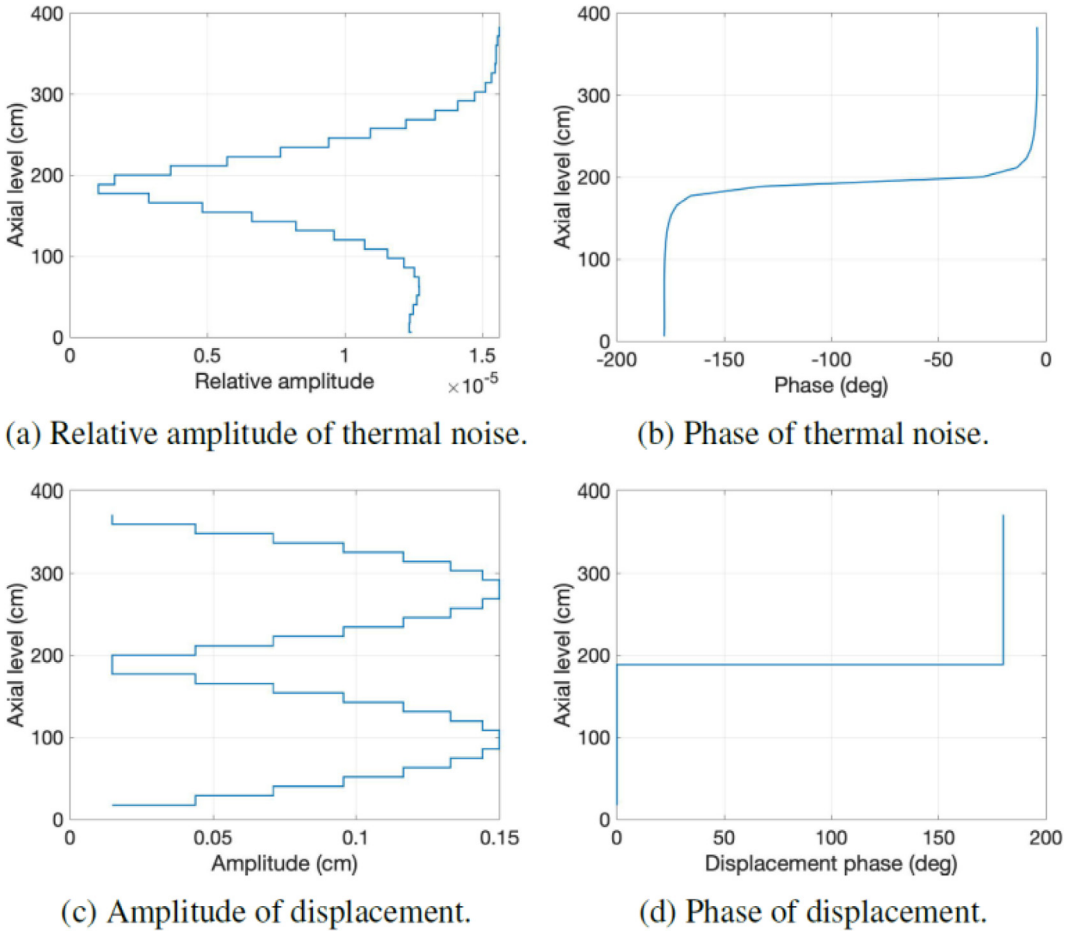

Fig. 14. Calculated axial thermal neutron noise for the FA located at the centre of the core (top) and prescribed axial perturbation associated with the vibrating FA (bottom).

extension, fuel assemblies. The latter approach is referred to as the fuel displacement model. Although the fuel displacement model seems like a more obvious modelling choice, a detailed study to confirm the validity of the delta gap model assumption was performed (Chionis, 2020; Chionis et al., 2020), and it is noted that only the delta gap model is compatible with S3K. To elaborate the delta gap model, when a FA moves δ mm in the positive x-direction, the surrounding water-gap increases by δ mm in the negative x-direction and decreases by δ mm in the direction of FA motion. The perturbed cross-sections resulting from the changes in water gap thicknesses are used to represent the vibrating fuel assemblies. As a limitation of the model, the execution of the incremental water gap in the lattice calculation is dependent on the lattice symmetry, i.e., only the nuclear data generated with the quarter and octant lattice symmetries are compatible with the downstream nodal codes. CASMO-5 does not perform an added branch calculation for the generation of cross sections corresponding to negative delta-gap widths for PWR fuel assemblies. The cross sections corresponding to the negative delta-gap widths are obtained in the latter steps at nodal level by means of extrapolation.

In the next step, CMS-LINK5 code collects all the nuclear data generated by the lattice and depletion calculations by CASMO-5 for every fuel segment, and post-processes them into a binary formatted library for further use by the nodal solvers, SIMULATE-3 and S3K. In SIMULATE-3, every FA is equally discretized into Z axial nodes, and every node is further split into 2x2 planar sub-nodes for a spatially precise solution. The cross-sections from CASMO-5 are homogenized within each such sub-node. The two-group 3D diffusion equation is solved for each sub-node using the two-group homogenized cross-sections, generated by CASMO-5, interpolated at the local operating conditions. In addition, the thermal–hydraulics model of SIMULATE-3 solves the total mixture mass, energy, and momentum equations for each FA. A core-follow calculation, evaluating the reactor state over one operational cycle is performed, and SIMULATE-3 stores the state points in 'restart files' for the transient nodal code S3K.

Lastly, SIMULATE-3 K, the three-dimensional two-group transient nodal code, reads the operating conditions of the core at the analysed core state via the respective restart file, and then initiates the transient full core calculation to calculate three-dimensional time-dependent two-group fluxes. The development of the improved modules of S3K and the set of supplementary MATLAB scripts was performed for modelling realistic scenarios of FA vibrations involving flexibility to impose different vibrational characteristics, modes and patterns to simultaneously vibrating fuel assemblies. The earlier version of the model and its evolution as well as study of various noise sources are described in previous works (Chionis, 2020; Chionis et al., 2020). In the improved assembly vibration model scheme, vibration of a central FA affecting the water gap widths between the two neighbouring fuel assemblies involves eight sub-nodes. To illustrate the model, a schematic diagram of the introduction of perturbed cross sections in the assembly vibration model in S3K is shown in Fig. 17. A central FA, FA_i, is displaced to the left direction, and the vibration is represented by introducing pre-calculated perturbed CASMO-5 cross sections corresponding to the modified water-gap width of $\delta/2$ in these eight affected sub-nodes, as marked in the Fig. 17.

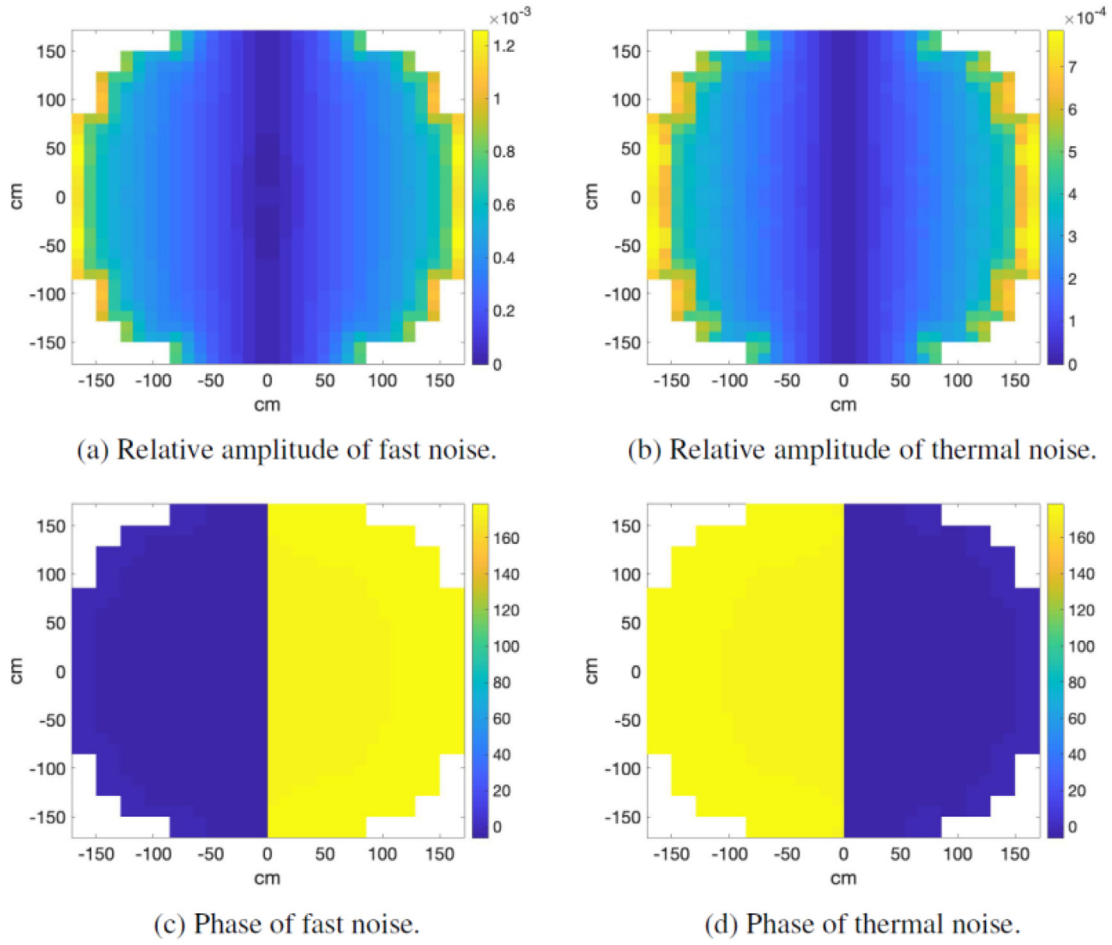

Fig. 15. Computed neutron noise induced by core barrel pendular vibration, at mid-elevation of the core.

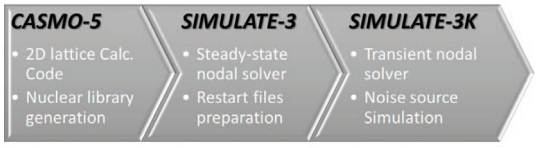

Fig. 16. Codes used in simulation of neutron noise.

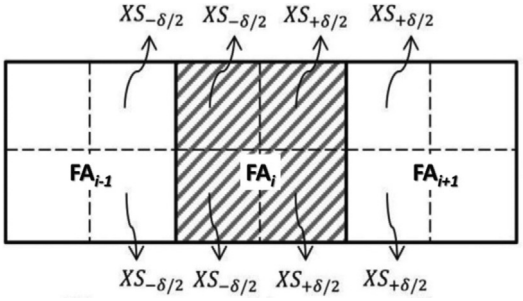

Fig. 17. Modification of cross sections when central FA, FA_i (striped), moves to the left direction. The modified cross sections, $XS_{-\delta/2}$ and $XS_{+\delta/2}$ are introduced in the eight labelled sub-nodes.

Perturbed cross-sections, $XS_{+\delta/2}$, corresponding to an increased water-gap width of $\delta/2$ are introduced in the four sub-nodes on the right, belonging to the oscillating assembly FA_i and the first neighbour, FA_{i+1}. Likewise, perturbed cross-sections, $XS_{-\delta/2}$, corresponding to a decreased water-gap width of $\delta/2$ are introduced in the four sub-nodes on the left belonging to FA_i and FA_{i-1} at a certain time step. The introduction of the cross-sections in such a way is essential to successfully model the displacement of FA_i towards FA_{i-1}, while ensuring that the fixed computational mesh in the core is conserved. The procedure is applied at every time step by appropriately modifying the delta gap widths between the involved fuel assemblies. As mentioned earlier, the perturbed cross-sections corresponding to the negative delta-gap widths that are missing in the pre-calculated CASMO-5 nuclear data, are obtained with S3K by extrapolating the values to delta gap width of δ. The maximum displacement amplitude of the fuel assemblies that can be modelled is limited by the distance between the neighbouring fuel assemblies.

In parallel, a set of supplementary PSI supporting MATLAB Scripts for Input Deck preparation (PSI-SMSID) were developed to facilitate the preparation of S3K input for simulating flexible and realistic FA vibrations. The scripts allow calculation of the time-dependent water gap widths between the chosen vibrating fuel assemblies and their adjacent assemblies; and generate support files to be included in the S3K calculation. A schematic diagram of the PSI-SMSID methodology including input parameters and features in support of S3K are shown in Fig. 18. It allows the user to input dynamic water-gap widths to S3K, corresponding to different vibrational patterns in terms of choice of vibrating assemblies, and vibrational characteristics such as amplitude, phase and frequency, etc., and patterns such as synchronized or unsynchronized vibrations. With the help of the supplementary scripts, the improved version of S3K lets the user impose any type of oscillation mode (e.g. random, stepwise, sinusoidal patterns, etc.) and vibrational

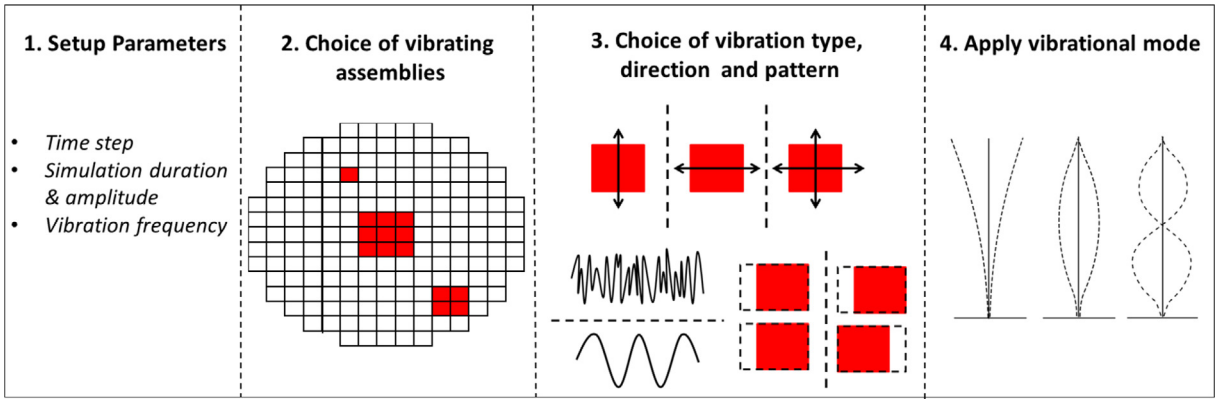

Fig. 18. PSI-SMSID Methodology to consolidate S3K in evaluating time-dependent delta gaps for vibrating fuel assemblies.

characteristics (i.e. amplitude and frequency) on both water gap width sides of the vibrating assembly by preserving its geometrical size. They also enable the user to impose pre-defined functions representative of the vibration modes of the fuel assemblies. This is done by creating an input vector of the axial shape by assigning factored coefficients between zero and one to each axial node. In other words, the FA is modelled to vibrate in a certain axial pattern by displacing each of the axial nodes by a width, δ, that is calculated using the coefficients and the water-gap widths at every time-step. With the external support file generated with the in–house MATLAB script containing the time-wise delta-gaps, S3K performs transient full core calculations to obtain three-dimensional time-dependent two-group fluxes. This modelling scheme enables S3K to replicate time-dependent realistic movements of the fuel assemblies and faithfully calculates the associated neutron noise in the core.

As the signals from the neutron detector locations in the core are limited, the nodal three-dimensional time-dependent neutron fluxes are also used to obtain the fast and thermal neutron noise amplitude and phase. The detection and localization of the vibrating fuel assemblies is based on the spectral analysis of the neutron detector signals. The methodology employs signal processing techniques involving a standard time- to frequency-domain analysis based on the Fourier transform of the autocorrelation function, which are implemented using MATLAB scripts. The detector signals are unfolded to reveal properties of the neutron noise source. The analysis includes radial and axial noise phenomenology based on the assessment of the auto power spectral densities (APSD) of the detector signals, and the phase and coherence between the azimuthal and axial neutron detectors. In the noise scenario of a FA vibration, a resonance peak is observed in the APSD at the excitation frequency, as well as an out-of-phase response between the signals belonging to the fuel assemblies located at opposite sides of the vibrating central FA (Verma et al., Jul. 2021). The presence of a phase difference of 180 degrees between the signals is in principle a characteristic feature, which can be used for localizing the source of oscillation in a system, in this case, a FA vibration. A deviation from the out-of-phase behaviour is typically seen when fuel assemblies are vibrating in peripheral locations, where large reactivity effects are present.

4.2. Numerical results

The results presented here are obtained for the four-loop Westinghouse 15x15 mixed core PWR of the OECD/NEA transient benchmark (Kozlowski and Downar, 2003). The neutron detectors are located at few discrete locations in the reactor as shown in the Fig. 19. A set of eight radial in-core neutron detectors are modelled at six axial locations each, and a set of four ex-core neutron detectors are modelled at two axial locations each.

Out of the various possible modes of FA vibrations, the most significant ones are the cantilevered mode at 0.6–2.0 Hz, where the FA is clamped-free at the top but fixed at the bottom, and the C-shaped and the S-shaped modes at 0.8–4.0 Hz and 5.0–10.0 Hz, respectively, where the FA is fixed at both the top and the bottom (Thie, 1981), as shown in Fig. 20.

Simulations are performed for noise scenarios based on the three modes of vibrations for a duration of 35 s at a time step of 0.01 s. For demonstration, a case of vibration of 5x5 central cluster of fuel assemblies is chosen to be modelled as synchronized pure sinusoidal vibrations in three vibrational modes along the x-direction with a maximum displacement amplitude of 0.1 cm. The fuel assemblies cluster are modelled to vibrate at 1.2 Hz for cantilevered mode and C-shaped mode, and at 5 Hz for S-shaped mode. The results are shown for relative noise distribution, calculated in terms of coefficient of variation (CV) in %. CV is defined as the ratio of the standard deviation to the mean value of the neutron flux in the energy group, obtained at any given node located at the core.

The relative noise distributions of the induced fast and thermal neutron noise are shown in Fig. 21, Fig. 22 and Fig. 23 for the vibration in cantilevered mode, C-shaped mode and S-shaped mode, respectively. The noise levels simulated by the in-core neutron detectors and the results from the spectral analysis are shown in Fig. 24, respectively, only for the case of vibrating assemblies in cantilevered mode.

The results show that the axial noise profiles in Fig. 21, Fig. 22 and Fig. 23 follow the imposed noise sources and reflect the predefined axial shape representative of the imposed vibrational modes. In case of the cantilevered mode vibration, higher neutron noise amplitude (1.8% and 2.5% for fast and thermal noise) is obtained at the core-top compared to the core-bottom (0.8% and 1% for fast and thermal) as the mode is modelled such that the FA is free to vibrate at the top while supported at the bottom by the core-support plate, which introduces much larger water gap widths at the top. The noise levels observed in the in-core neutron detectors in Fig. 24(a) confirm the behaviour. In case of the C-shaped mode, the core-lower and -upper support plates offer resistance to the vibrations of assemblies from the bottom and the top, and introduces wider water-gap widths in the middle, which is reflected in the induced noise. In case of the S-shaped mode, the time-dependent vibration of the FA is reflected in the noise distribution, as it appears to be split into two symmetric halves axially, representative of the S-shaped noise source. In general, the neu-

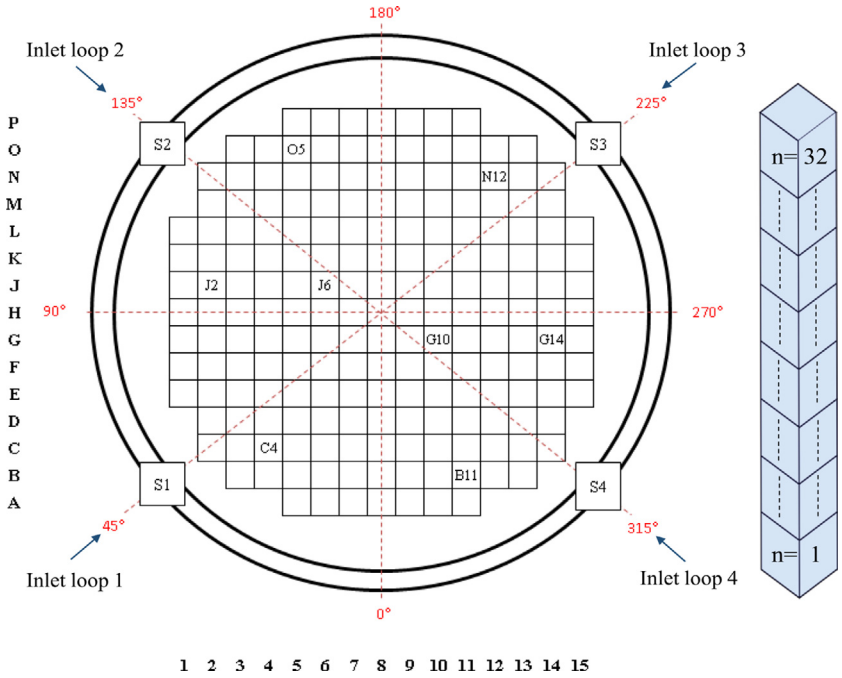

Fig. 19. Left: Radial layout of the OECD-PWR core model along with the labelled locations of the in-core, ex-core neutron detectors and the coolant loops. Right: Axial cross section of a FA with 32 nodes.

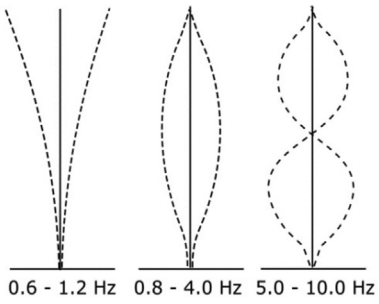

Fig. 20. FA vibrational modes and associated frequency ranges.

tron noise amplitude is slightly higher at the top-half compared to the bottom-half due to the more negative moderator temperature coefficient of reactivity at the top.

It is found that for all the three scenarios of FA vibrations, the neutron noise distribution is symmetric around the oscillating fuel assemblies. For illustrative purposes, the radial distribution of the relative noise is only shown for cantilevered mode, as seen in Fig. 21. In case of a vibrating cluster of assemblies, the relative movement of the central FA is zero compared to the rest of the moving cluster. This is understood from the way perturbed cross sections are introduced at the level of S3K, as illustrated in Fig. 17 previously. The vibration of the FA to the left and to the right effectively cancels the perturbed cross sections of the central FA. Therefore, the induced noise at the centre of the source is almost zero, while the highest noise amplitude is obtained in the adjacent fuel assemblies and the peripheral assemblies of the vibrating cluster, along the direction of motion, as these assemblies are impacted the most from the water-gap modification. The noise decreases significantly a few mean free paths away from the noise source. For a randomly vibrating FA cluster, the behaviour is modified slightly, and the noise amplitude is distributed uniformly in all the directions radially. The neutron noise behaviour is qualitatively consistent in both energy groups, however, the fast neutron noise is observed to be more diffused in the core due to the relatively larger mean free path of fast neutrons as compared to thermal neutrons. The thermal noise has higher amplitude because of the higher relative impact on the absorption cross sections due to changes in the water gap widths.

It is also confirmed that the phase response of the induced neutron noise due to vibration of the central cluster is out-of-phase between the two halves of the symmetric core, as expected. Further, spectral analysis of the induced neutron noise in the frequency domain reveals that the excitation frequencies of the vibrating fuel assemblies in cantilevered mode are observable in the noise spectrum at 1.2 Hz (excitation peak), as shown in Fig. 24(b).

Finally, for the sake of brevity, only a few illustrative examples are included in this section to demonstrate the capabilities of the model based on S3K. Another possible source of mechanical vibration noise is core barrel vibration, which is modelled as collective vibration of all the fuel assemblies in the core (Verma et al., Jul. 2021; Vidal-Ferràndiz et al., 2020). As the core barrel is vertically suspended from the core-top, the noise source is modelled as simultaneous vibrations of fuel assemblies clamped from the top and moving freely at the bottom, similar to the cantilevered vibrational mode of a 5x5 cluster of fuel assemblies, presented above.

5. Modelling strategy with KMACS-ATHLET-QUABOX-CUBBOX

5.1. Model description

Another strategy to investigate core barrel vibrations in a nuclear reactor, similar to the methodology described in Section 4, is to simulate the variations of the water gap between the outermost fuel element row and the core baffle as a simple model of collective, coherent fuel element motions or core barrel vibrations. In addition to the reaction of the core to different frequencies, the dependence on the burn-up state of the reactor was investigated. The reactor core investigated is a German 4-loop pre-Konvoi PWR containing 193 fuel assemblies with a 16x16 lattice.

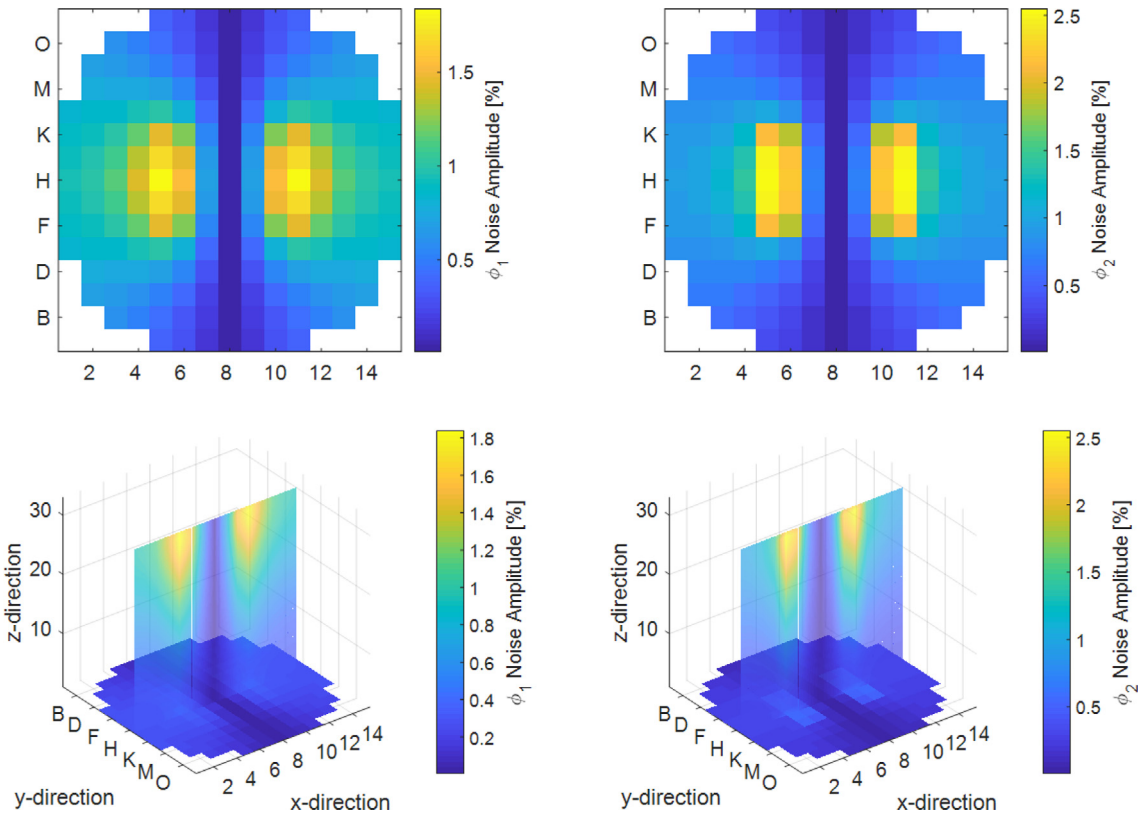

Fig. 21. Radial (top) and axial (bottom) distributions of the fast (left) and thermal (right) induced neutron noise due to vibration of the 5 × 5 central FA cluster in x-direction in the cantilevered mode at 1.2 Hz. The radial distributions are obtained at the axial node where noise level is the highest.

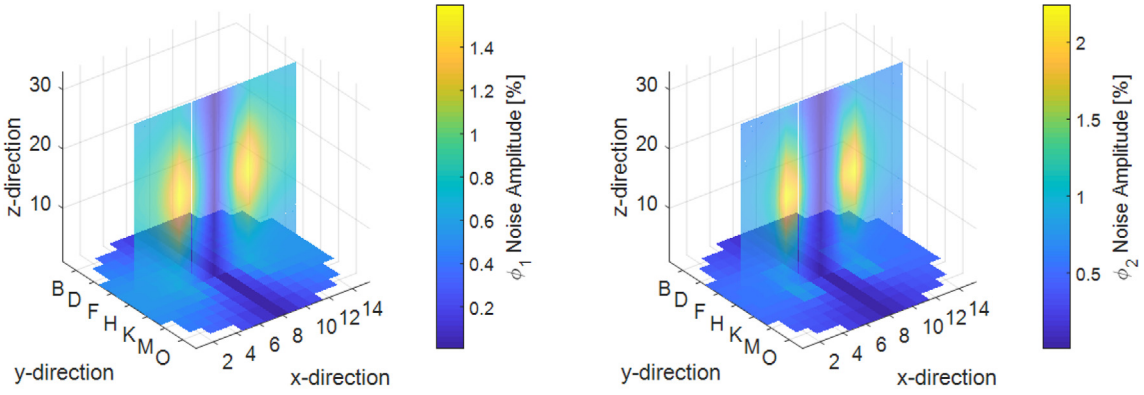

(a) (b)

Fig. 22. Axial distributions of the fast (a) and thermal (b) induced neutron noise due to vibration of the 5 × 5 central FA cluster in x-direction in the C-shaped mode at 1.2 Hz.

The numerical simulations of neutron noise shown in this section have been performed using a customized developer version of the GRS in-house core simulator KMACS. KMACS follows a typical two-step approach:

- First, the neutron physical properties of fuel assemblies are precalculated in an infinite lattice for discrete energy groups and a set of thermal–hydraulics and burnup states covering the expected reactor conditions.
- The second step is the core cycle calculation, which is an iterative process. During this phase, the core is simulated based on the nuclear data generated in the first step using a nodal neutron kinetics solver coupled to a thermal–hydraulics code. The calculated neutron flux then serves as input to a burnup module, which updates the nodal core burnup state. This code sequence is repeated for each burnup point.

KMACS delegates the aforementioned tasks to specialised backend codes for which it provides input generation, code execution and data management facilities. In this study, the NEWT code from the SCALE package by ORNL (version 6.2.2) is used for macroscopic cross section generation. The neutron flux distribution is simulated by the coupled code ATHLET-QUABOX/CUBBOX. ATHLET-QUABOX/CUBBOX is also used for transient simulations in this study. ATHLET, a best-estimate thermal–hydraulics system code from the AC^2 package, and QUABOX/CUBBOX, a 3D nodal diffusion solver, are both being developed by GRS.

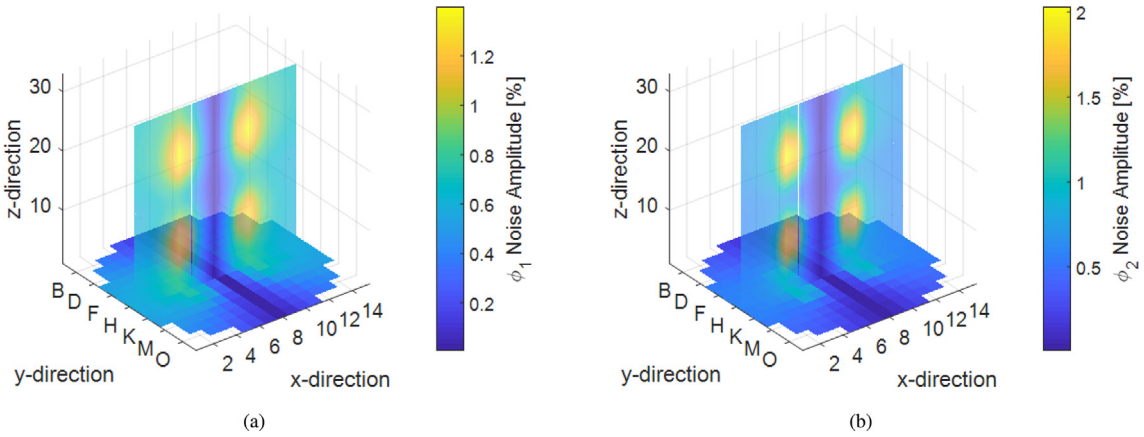

Fig. 23. Axial distributions of the fast (a) and thermal (b) induced neutron noise due to vibration of the 5 × 5 central FA cluster in x-direction in the S-shaped mode at 5 Hz.

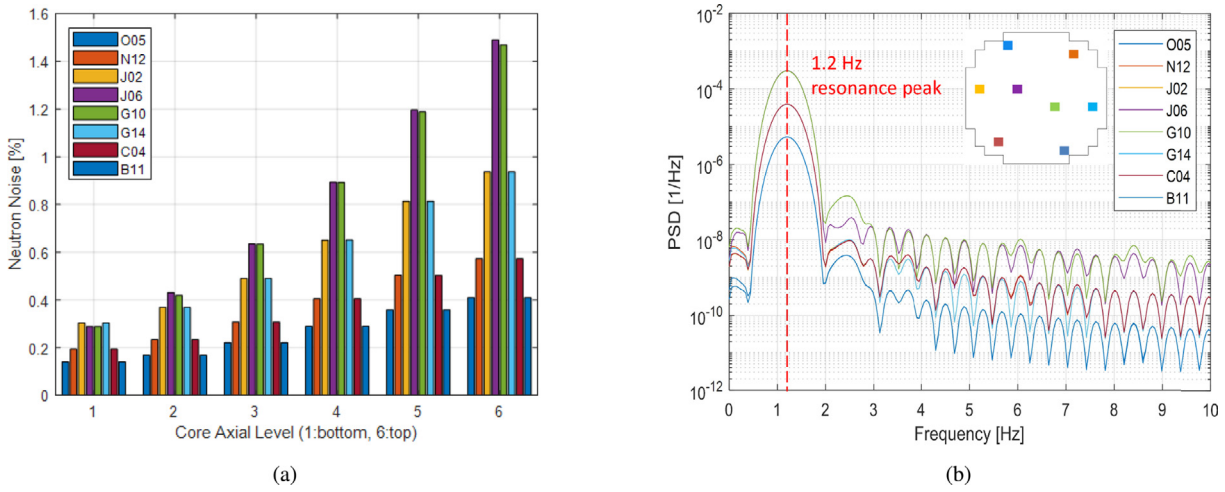

Fig. 24. (a) Noise levels in in-core neutron detectors for the cantilevered vibration mode and (b): Power spectral densities obtained with in-core neutron detectors for the cantilevered vibration mode. The dashed red line represents the excitation frequency of the vibrating fuel assemblies.

Since neither QUABOX-CUBBOX nor ATHLET currently provide models for dynamic geometry, two main technical extensions were implemented in the coupled code-system ATHLET-QUABOX/CUBBOX.

First, the water gap size dependence was encoded into the macroscopic radial reflector cross-sections by varying the respective geometry in the lattice calculations and by introducing the gap width as an additional dimension into the nuclear data tables already parametrized by boron concentration and moderator density.

Second, in order to control the spatial distribution and the temporal evolution of the water gaps, a two-dimensional mapping was added to the ATHLET input which assigns the water gap width as boundary condition to a given radial reflector assembly positions. The interface between ATHLET and QUABOX-CUBBOX was extended, so that the water gap width could be communicated to the flux solver and then be used as part of the reactor state in the interpolation of the nuclear cross-sections at runtime. A schema of the approach is depicted in Fig. 25.

5.2. Results

5.2.1. Steady-state calculations

A complete cycle was simulated with KMACS. Each burn-up point was saved and the conditions at Beginning Of Cycle (BOC), Middle Of Cycle (MOC) and End Of Cycle (EOC) serve as starting points for transient calculations with ATHLET/QUABOXCUBBOX.

The results of the KMACS cycle calculation were verified against a SIMULATE reference calculation. The maximum deviation between the two models for the critical boron concentration during the whole cycle is below 14 ppm, which is satisfactory, thus validating the KMACS model under nominal conditions.

Next, the nuclear data for the radial reflector were recalculated for several water gap widths ranging from zero to the maximal achievable space of about 2.6 cm in the fuel element row containing the most elements. The resulting curves for the absorption (Σ_a) and the total (Σ_t) cross-sections are shown in Fig. 26 for nominal thermal–hydraulic conditions. Nonlinear behaviour can be observed starting around 1 cm.

5.2.2. Transient calculations

Two functions governing the gap widths were respectively assigned to the southern and northern halves of the reactor. The two functions are 180 degrees phase-shifted sinusoid functions. The amplitude depends on the maximal achievable gap width in a given assembly row, i.e. 2.6 cm for the first and last rows. This (unrealistic) assumption was made in order to maximize the flux changes caused by the geometry variations.

Unfortunately, the gap variations could not be fully constrained to horizontal gaps due to model constraints: QUABOX-CUBBOX

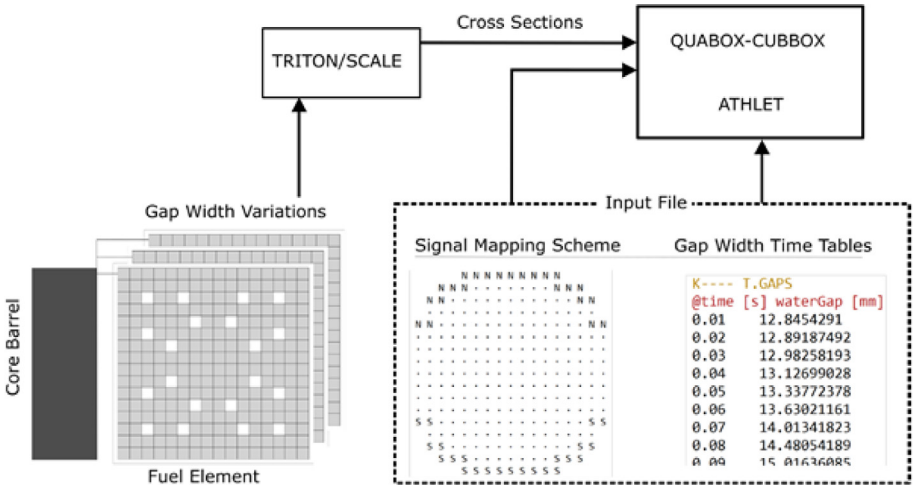

Fig. 25. Schematic representation of the modelling approach.

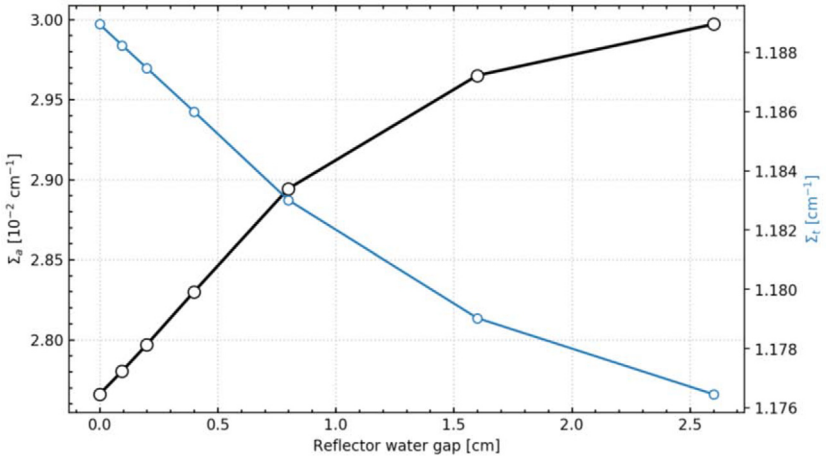

Fig. 26. Water gap size dependence of the absorption and total cross-sections in the radial reflector.

does not support anisotropic assembly discontinuity factors. This is also the reason why no attempt was made to extend the model to the analysis of vibrating fuel assemblies away from the reflector. Therefore, if a reflector assembly whose cross sections are dynamically changed to reflect the time-dependence of the north/south water gap width also has an east/west neighbour, in effect the water gaps are modified in both directions.

The following results were taken from a horizontal plane in the middle of the reactor and a node located at the northern reflector. The shape of the time evolution of the thermal flux in the measurement node was plotted against the gap signal in Fig. 27 for an excitation frequency of 0.8 Hz. It can be observed that the general shape of the two functions appears to be the same, and that the flux slightly lags behind the driving force.

As expected from experimental reactor measurements, Fig. 28 exhibits the rise of the amplitude of flux variations during a burn-up cycle from the BOC over the MOC to the EOC. Compared to BOC, the amplitude increased at MOC by a factor of 1.4 and by 2.1 at EOC.

To analyse the frequency domain of the thermal flux signal, the Auto Power Spectral Density (APSD) was calculated for each of the three cycle time points (Fig. 29). A peak is clearly visible at the excitation frequency ω_p (0.8 Hz). As the burnup increases, so does the maximum of this peak. Aside from the excitation frequency, the data for BOC and MOC show the occurrence of a weakly developed second maximum at $2\omega_p$ which could be caused by non-linear effects. At MOC and EOC, this second maximum can barely be discerned because of the different scale of the y-axis.

When the excitation frequency is increased to 8 Hz, not only does a higher harmonic frequency appears in the spectrum, but in addition, a peak at an intermediate frequency is observed (Fig. 30). The trend, that the first peak increasingly dominates the spectrum towards the end of the cycle, can also be found for 8 Hz. Further studies are needed to rule out numerical as well as model artefacts and to thus corroborate the interpretation of higher order frequencies.

Finally, an overview of the spatial distribution of the induced fluctuations in the thermal flux, expressed as the difference between the maximum and minimum value in each node, is given in Fig. 31. The amplitude amounts to 0.74% of the static flux (nominal gap widths) in the measurement node and reaches a maximum of 1.98% in the lateral nodes of the bottom and topmost rows, in which the effect is overestimated due to the unwanted east–west gap variation described earlier.

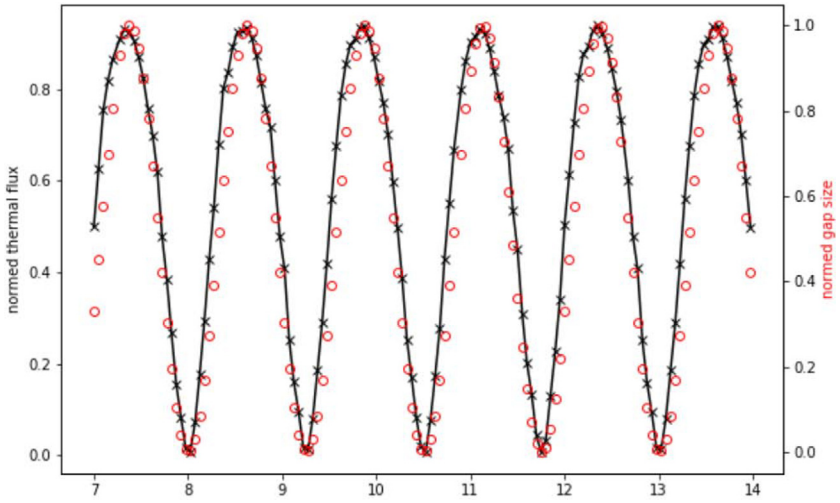

Fig. 27. Comparison of the time evolution of the thermal flux compared to the gap signal.

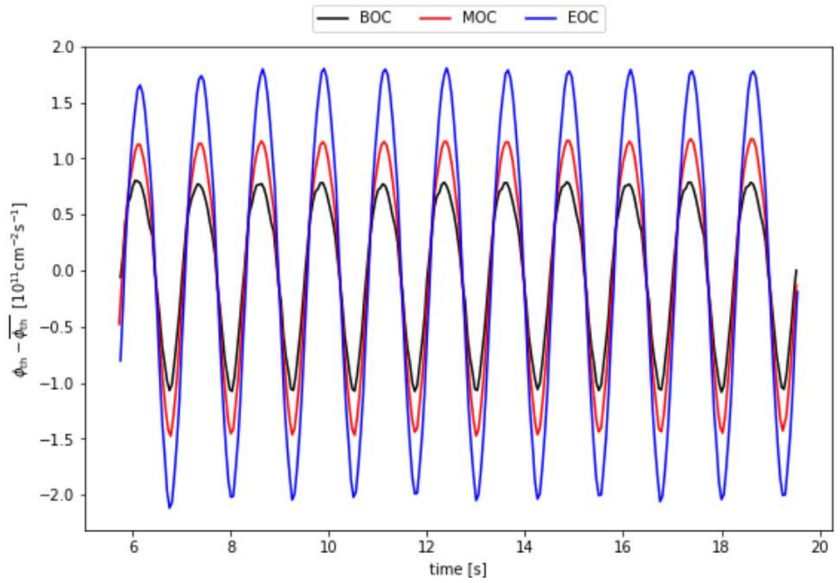

Fig. 28. Increase of the flux variations with cycle burn-up.

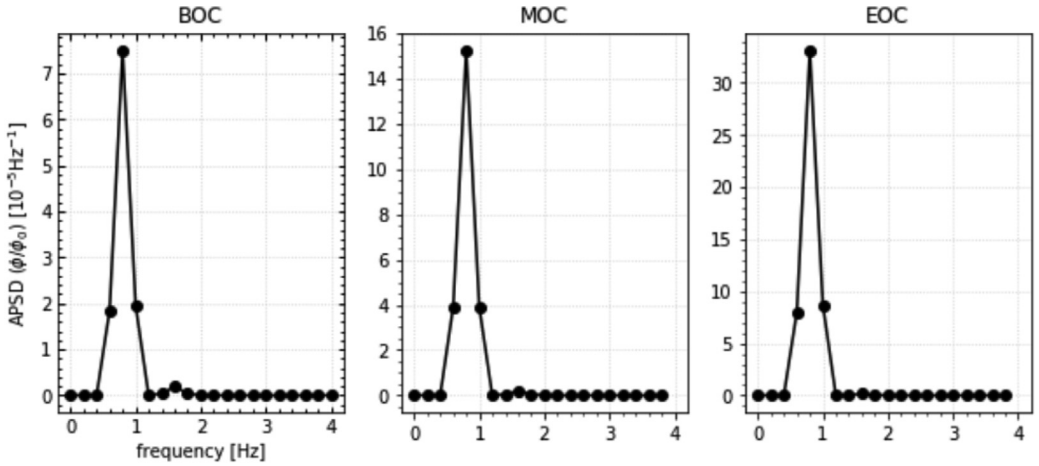

Fig. 29. Power spectral density of the thermal flux normed by the static flux (0.8 Hz). The y-axes have different scales.

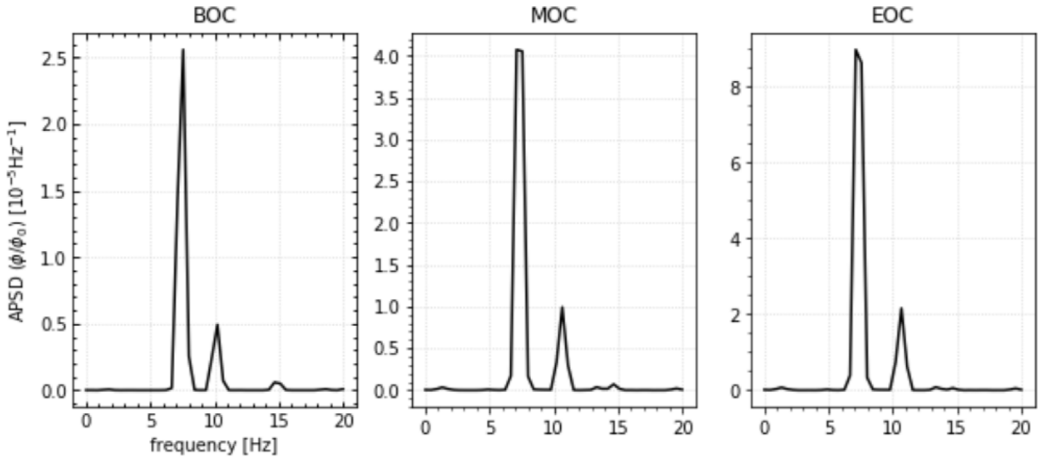

Fig. 30. Power spectral density of the thermal flux normed by the static flux (8 Hz). The y-axes have different scales.

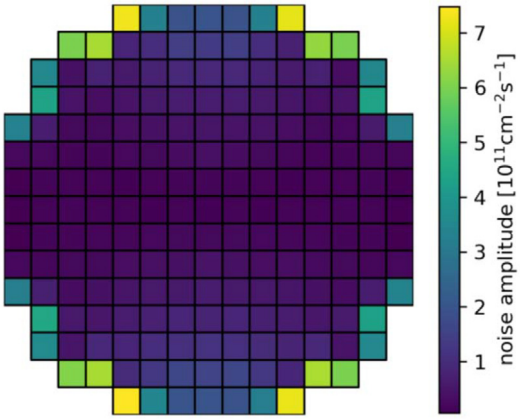

Fig. 31. Spatial distribution of the difference between maximum and minimum induced flux in each node of the middle horizontal layer.

6. Conclusions

In this work, different types of methodologies for the study of the influence of the mechanical vibrations of fuel assemblies on the neutron flux in reactor core, have been discussed. These methodologies employ the diffusion approximation to simulate the neutron noise in the time or the frequency domain. The diffusion-based approach is expected to be less accurate in the vicinity of the vibrating fuel assemblies, but correct when considering distances larger than a few diffusion lengths away from the perturbation. All methodologies provide consistent results and can reproduce typical features of the neutron noise induced by mechanical vibrations of core components. The neutron noise related to the fast energy group has a more extensive spatial impact in the reactor core because of the larger mean free paths of fast neutrons. Spectral analysis of the neutron noise in the frequency domain shows that the main frequency of the neutron noise corresponds to the fundamental frequency of the mechanical vibrations.

First, FEMFFUSION can perform simulations in both the time and frequency domains. The efforts have been centred on showing the consistency between the time domain and the frequency domain calculations. Numerical results identify two different effects in the neutron field caused by the FA vibration. First, a global slow variation of the power is observed because of a change in the criticality of the system. This effect is small and would be compensated by reactivity feedback mechanisms in a real reactor. Second, an oscillation of the neutron flux with the same frequency as the assembly mechanical vibration is demonstrated. The corresponding neutron noise is highly spatially dependent. For this second effect, a very close agreement between the time domain and the frequency domain approach is found.

Second, CORE SIM + can be used to study various neutron noise scenarios in realistic three-dimensional reactor configurations. Its numerical scheme in the frequency domain allows building accurate models of neutron noise sources and to perform reactor neutron noise calculations in an optimized manner, at a relatively cheap computational cost. Examples of vibrations of fuel assemblies and core barrel in a PWR were analysed.

The third methodology is centred on using commercial codes as CASMO-5, SIMULATE-3 and SIMULATE-3K. This methodology allows time-domain simulations of the neutron noise induced by different neutron noise sources in a nuclear reactor. In particular, the modelling of fuel assembly vibrations is based on the perturbation of the macroscopic cross-sections that is obtained from the variation of the water gap of the vibrating fuel assemblies. Thermal–hydraulic feedback effects are also included in the simulations. Using this methodology, the characteristics of neutron noise due to different vibration modes of fuel assemblies, with and without additional fluctuations of coolant temperature and flow, can be investigated.

Finally, a model for time-dependent geometry was implemented for the code system ATHLET/ QUABOX-CUBBOX employing a cross-section-based approach for encoding water gap width variations at the reflector to model core barrel vibrations. The approach suffers from several limitations, the main one being the isotropic treatment of assembly discontinuity factors in QUABOX-CUBBOX, which induces an unwanted variation of the east–west gap width while simulating north–south vibration and also prevents the use of this model to the analysis of vibrating fuel assemblies away from the reflector. In view of these shortcomings, the applicability of the approach may be restricted to the study of qualitative behaviour. Nevertheless, this approach has its advantages since it allows examining the effects of cycle burn-up and to combine the analysis with thermal–hydraulic feedback models and noise sources. Moreover, results from advanced mechanical models can be incorporated. Further analyses will have to chart the applicability and explanatory power of this numerical model.

As future lines of investigation, there is the need to compare these models and study the differences in operating nuclear reactors. Also, it must be investigated the validity and limitations of diffusion theory when analysing real neutron noise scenarios.

Finally, some improvements in the modelling of neutron noise sources are needed because the work done so far is focused on PWRs and future efforts should also consider the modelling of neutron noise in other type of reactors.

CRediT authorship contribution statement

A. Vidal-Ferràndiz: Methodology, Software, Validation. **D. Ginestar:** Methodology, Validation. **A. Carreño:** Methodology, Software. **G. Verdú:** Methodology, Validation. **A. Dokhane:** Methodology, Software, Validation. **V. Verma:** Methodology, Software, Validation. **Y. Perin:** Methodology, Software, Validation. **J. Herb:** Methodology, Software, Validation. **A. Mylonakis:** Methodology, Software, Validation. **C. Demazière:** Conceptualization, Methodology, Software, Validation. **P. Vinai:** Conceptualization, Methodology, Software, Validation.

Declaration of Competing Interest

The authors declare that they have no known competing financial interests or personal relationships that could have appeared to influence the work reported in this paper.

Acknowledgements

The research conducted was made possible through funding from the Euratom research and training programme 2014–2018 under grant agreement No. 754316 for the "CORe Monitoring Techniques And EXperimental Validation And Demonstration (CORTEX)" Horizon 2020 project, 2017–2021.

References

Balay, S., Abhyankar, S., Adams, M.F., Benson, S., Brown, J., Brune, P., Buschelman, K., Constantinescu, E.M., Dalcin, L., Dener, A., Eijkhout, V., Gropp, W.D., Hapla, V., Isaac, T., Jolivet, P., Karpeev, D., Kaushik, D., Knepley, M.G., Kong, F., Kruger, S., May, D.A., McInnes, L.C., Mills, R.T., Mitchell, L., Munson, T., Roman, J.E., Rupp, K., Sanan, P., Sarich, J., Smith, B.F., Zampini, S., Zhang, H., Zhang, H., Zhang, J., 2021. PETSc Web page. URL:https://petsc.org/.

Carreño, A., Vidal-Ferràndiz, A., Ginestar, D., Verdu, G., 2021. Adaptive time-step control for modal methods to integrate the neutron diffusion equation. Nucl. Eng. Technol. 53 (2), 399–413.

Carreño, A., Vidal-Ferràndiz, A., Ginestar, D., Verdú, G., 2022. Frequency-domain models in the SPn) approximation for neutron noise calculations. Prog. Nucl. Energy 148, 104233.

Chionis, D., 2020. Development of advanced methodologies for monitoring and modelling of neutron noise in modern lwr cores. Ph.D. thesis, PhD Thesis, EPFL, Switzerland.

Chionis, D., Dokhane, A., Belblidia, L., Ferroukhi, H., Girardin, G., Pautz, A., 2020. Development and verification of a methodology for neutron noise response to fuel assembly vibrations. Ann. Nucl. Energy 147, 107669.

Cronin, J., Smith, K., Planck, D.V., 1995. SIMULATE-3 methodology. Tech. rep., Studsvik Scandpower, Nyköping, Sweden, SSP Technical Report SOA-95/18 – Rev 0.

Demazière, C., 2006. Analysis methods for the determination of possible unseated fuel assemblies in bwrs. Int. J. Nucl. Energy Sci. Technol. 2 (3), 167–188.

Demazière, C., 2011. CORE SIM: A multi-purpose neutronic tool for research and education. Ann. Nucl. Energy 38 (12), 2698–2718.

Demazière, C., Andhill, G., 2005. Identification and localization of absorbers of variable strength in nuclear reactors. Ann. Nucl. Energy 32 (8), 812–842.

Demazière, C., Dokhane, A., 2019. Deliverable 3.1: Description of scenarios for the simulated data. Tech. rep., CORTEX project. URL: https://cortex-h2020.eu/wp-content/uploads/2019/07/CORTEX_D3_1_Description_of_scenarios_for_the_simulated_data_V1.pdf.

Demazière, C., Pázsit, I., 2009. Numerical tools applied to power reactor noise analysis. Progr. Nucl. Energy 51 (1), 67–81.

Demazière, C., Vinai, P., Hursin, M., Kollias, S., Herb, S., 2018. Overview of the cortex project. In: Proceedings of international conference on physics of reactors – PHYSOR 2018: Reactor physics paving the way towards more efficient systems. Cacún, México, pp. 2917–2980.

Ferguson, D.R., Derstine, K.L., 1977. Optimized iteration strategies and data management considerations for fast reactor finite difference diffusion theory codes. Nucl. Sci. Eng. 64 (2), 593–604.

Ferrer, R., 2015. CASMO-5 methodology manual. Tech. rep., Studsvik Scandpower, Nyköping, Sweden, SSP Technical Report SSP-08/405 – Rev. 4.

Fry, D., March-Leuba, J., Sweeney, F., 1984. Use of neutron noise for diagnosis of in-vessel anomalies in light-water reactors. Oak Ridge National Lab. Tech. rep.

Gammicchia, A., Santandrea, S., Zmijarevic, I., Sanchez, R., Stankovski, Z., Dulla, S., Mosca, P., 2020. A MOC-based neutron kinetics model for noise analysis. Ann. Nucl. Energy 137, 107070.

Gill, D., Asmy, Y., 2009. A jacobian-free newton-krylov iterative scheme for criticality calculations based on the neutron diffusion equation. In: Int. Conf. on Advances in Mathematics, Computational Methods, and Reactor Physics (M&C 2009). Saratoga Springs, NY, USA, pp. 1–15.

Grandi, G., 2011. SIMULATE-3K models & methodology. Tech. rep., Studsvik Scandpower, Nyköping, Sweden, SSP Technical Report SSP-98/13 – Rev. 7.

Hébert, A., 1985. Application of the hermite method for finite element reactor calculations. Nucl. Sci. Eng. 91 (1), 34–58.

Kozlowski, T., Downar, T., 2003. Oecd/nea and us nrc pwr mox/uo2 core transient benchmark. Tech. rep., OECD Nuclear Energy Agency Nuclear Science Committee.

Malmir, H., Vosoughi, N., 2015. Propagation noise calculations in vver-type reactor core. Prog. Nucl. Energy 78, 10–18.

Mylonakis, A., Vinai, P., Demazière, C., 2021. CORE SIM+: A flexible diffusion-based solver for neutron noise simulations. Ann. Nucl. Energy 155, 108149.

Mylonakis, A.G., Vinai, P., Demazière, C., 2020. Numerical solution of two-energy-group neutron noise diffusion problems with fine spatial meshes. Ann. Nucl. Energy 140, 107093.

Park, J., Lee, J.H., Kim, T.-R., Park, J.-B., Lee, S.K., Koo, I.-S., 2003. Identification of reactor internals' vibration modes of a korean standard pwr using structural modeling and neutron noise analysis. Prog. Nucl. Energy 43 (1–4), 177–186.

Pázsit, I., 1977. Investigation of the space-dependent noise induced by a vibrating absorber. Atomkernenergie 30, 29–35.

Pázsit, I., Demazière, C., 2010. Noise techniques in nuclear systems. In: G., C.D. (Ed.), Handbook of Nuclear Engineering. Springer, Boston, MA, pp. 1629–1737.

Rouchon, A., 2016. Analyse et développement d'outils numériques déterministes et stochastiques résolvant les équations du bruit neutronique et applications aux réacteurs thermiques et rapides. Ph.D. thesis, Université Paris-Saclay.

Seidl, M., Kosowski, K., Schüler, U., Belblidia, L., 2015. Review of the historic neutron noise behavior in german kwu built pwrs. Prog. Nucl. Energy 85, 668–675.

Thie, J., 1981. Power Reactor Noise. American Nuclear Society, Massachusetts.

Verma, V., Chionis, D., Dokhane, A., Ferroukhi, H., Jul. 2021. Studies of reactor noise response to vibrations of reactor internals and thermal-hydraulic fluctuations in PWRs. Ann. Nucl. Energy 157, 108212.

Verma, V., Demazière, C., Vinai, P., Ricciardi, G., Jacqmin, R., 2019. Assessment of the neutron noise induced by stationary fuel assembly vibrations in a light water reactor. In: Int. Conf. on Mathematics and Computational Methods applied to Nuclear Science and Engineering (M&C 2019). Portland, Oregon, USA, pp. 1–10.

Vidal-Ferràndiz, A., Carreño, A., Ginestar, D., Demazière, C., Verdú, G., 2020. A time and frequency domain analysis of the effect of vibrating fuel assemblies on the neutron noise. Ann. Nucl. Energy 137, 107076.

Vidal-Ferràndiz, A., Carreño, A., Ginestar, D., Verdú, G., 2021. FEMFFUSION a finite element method code for nuclear reactor modelling. URL: https://femffusion.webs.upv.es/, accessed: 2021-12-20.

Vidal-Ferràndiz, A., Fayez, R., Ginestar, D., Verdú, G., 2014. Solution of the lambda modes problem of a nuclear power reactor using an h–p finite element method. Ann. Nucl. Energy 72, 338–349.

Vidal-Ferràndiz, A., Fayez, R., Ginestar, D., Verdú, G., 2016. Moving meshes to solve the time-dependent neutron diffusion equation in hexagonal geometry. J. Comput. Appl. Math. 291, 197–208.

Vidal-Ferràndiz, A., Demazière, C., Ginestar, A.D.D., Knospe, A., Kuentzel, M., Mylonakis, A., Périn, Y., Lange, C., Verdú, G., Verma, V., Vinai, P., 2020. Deliverable 1.3: Modelling of neutron flux response to vibrating fuel assemblies. Tech. rep., CORTEX project,https://cortex-h2020.eu/wp-content/uploads/2021/03/CORTEX_D1_3_Modelling_of_the_neutron_flux_response_to_vibrating_fuel_assemblies_V1.pdf.

Yamamoto, T., 2013. Monte carlo method with complex-valued weights for frequency domain analyses of neutron noise. Ann. Nucl. Energy 58, 72–79.